

Space Shuttle Early Reentry



In this example we will analyze the Space Shuttle Orbiter and design a flight control system during early atmospheric entry from space. In early reentry the dynamic pressure is low, in the order 2 to 10 psf, and the vehicle is flying at hypersonic speeds Mach 20 to 27 and at high angles of attack for speed-breaking. Prior to reentry and at an altitude above 400,000 feet the vehicle ignites the orbital maneuvering engines to reduce its orbital speed and to allow gravity to take effect. Then it maneuvers using the RCS jets and the angle of attack is controlled by the RCS at approximately 40° before entering into the atmosphere with a shallow flight path angle. The vehicle also banks at approximately 80° to ensure atmospheric penetration and to avoid bouncing back off into space. Precise control of the angle of attack (α) is very important during early entry because (α) regulates the heat dissipation caused by atmospheric friction. The angle of attack also controls the flight path angle γ which is initially shallow, at -0.85° to avoid overheating. Controlling (α) and (γ) is very important during early reentry because if the flight path angle is too shallow the vehicle will bounce back into space. If it is too steep it will overheat and burn. The guidance system uses a pre-selected alpha reference as a function of the relative velocity to manage temperature and to assure a steady and safe heat dissipation rate. The lateral guidance dissipates excess kinetic energy by performing roll maneuvers (S-turns) as necessary to control the down-range and cross-range position all the way to landing. During roll maneuvering the orbiter rolls about the velocity vector V_0 in order to minimize the beta angle and side

loads. As the vehicle descends to lower altitudes the angle of attack is reduced from 40° mainly by adjusting the positions of the elevons and the body-flap to smaller values and the vehicle switches to normal acceleration (N_z) control mode. After a period of about 30 minutes from initial entry the vehicle glides down to earth and lands unpowered on a runway.

The aero-surfaces that control the Shuttle orbiter are: two inboard and two outboard elevons, body-flap, rudder, and speed-brake. The pitch direction and angle of attack is controlled mainly by deflecting the inboard elevons. The elevons and the body-flap are trimmed to positions that attain the required angle of attack which regulates speed-breaking. The RCS is controlled by a separate feedback loop to maintain the required attitude especially at very low dynamic pressures. The body-flap is not active in the control loop but it is scheduled as needed for trimming and to provide good elevon effectiveness. The speed-brake is used near landing. During early reentry when the dynamic pressure is below 4 psf and the aero-surfaces are not very effective the vehicle is controlled by combining RCS and aero-surfaces. The RCS activity is gradually phased out as the dynamic pressure increases, although it is not completely eliminated to guard against lateral uncertainties in the aero-surface coefficients, especially in flight conditions which are sensitive to aileron (LCDP) reversals.

There is also a phugoid mode that causes dynamic coupling between the angle of attack, altitude, and velocity. The phugoid mode is a low frequency, low-damped, roller-coaster type of oscillation which is created by an exchange between potential and kinetic energy. The phugoid oscillation is slightly dampened by applying normal acceleration (N_z), and N_z -integral feedback. An early Shuttle reentry flight condition was selected in this example to demonstrate how to blend control surfaces with RCS jets and to demonstrate a multi-level, pulse-width-modulation thrusting logic. The analysis is separated in 3 sections. In Section 1 we generate rigid vehicle models, design flight control laws, derive mixing logic that combines the aero-surfaces and also a jet firing logic for the RCS. We analyze stability and develop simulation models to test our design. In section 2 we introduce structural flexibility in the vehicle models, select a set of 50 modes, include aero-elasticity, analyze system stability in the frequency domain, and upgrade the simulation by including flexibility. In Section 3 we will repeat the stability analysis in the z-domain and develop simulation models using discrete systems.

1.0 Rigid Body Analysis

For rigid body control design we must first develop separate vehicle models for pitch and lateral axes control synthesis. The flight control laws consist of gain feedback alone without flexibility compensation, which will be added in Section 2. We will also create a vehicle model that will be used in Matlab to perform frequency domain stability analysis and time-domain simulations. This system includes both pitch and lateral coupled dynamics. Actuator and sensor dynamics are not included in this section. They will be introduced in Section 2 during flex vehicle analysis.

1.1 Rigid Body Vehicle Models

For rigid body analysis we will create two vehicle state-space models: a vehicle model for control design with output rates which are defined in stability axes, and a body axes model for analysis and time domain simulations. The x-axis in the stability axis model is defined to be along the velocity vector V_0 . Roll rate is about V_0 and the yaw rate is orthogonal to pitch and roll. The lateral gains derived (using the LQR method) are based on this model because the roll guidance command on the vehicle is defined about the velocity vector V_0 in order to minimize the side loading.

The data files for this analysis are in folder “C:\Flixan\Examples\Shuttle Hypersonic Re-Entry\Rigid_Body”, and the input data file is “Shuttle_Entry_RB.inp”. The vehicle data title for the stability axes model is: “Shuttle Early Hypersonic Re-Entry, Rigid Stabil Axes Model for LQR”, and the vehicle data title for the body axes simulations model is: “Shuttle Early Hypersonic Re-Entry, Rigid Body Axes Model for Simulation”. The stability axes option is defined in the vehicle input data-set in the flags line, which is the line below the title and comments, by setting it to “Stability Axes Output” flag, instead of “body axes” which is the default option. The “With Turn Coordination” flag is also set on in the flags line, only in the stability axis control design vehicle data-set, because we assume that the vehicle control system includes an aileron/ rudder turn coordination system that balances the side forces during turns. In other words the design model rolls about V_0 and includes the roll to yaw turn-coordination coupling in the vehicle dynamics.



Now let's take a look at some of the vehicle parameters in the input data file “Shuttle_Entry_RB.Inp”. The vehicle is reentering at Mach 25, with a velocity of 18,640 (ft/sec), at an altitude 245,000 (ft), an angle of attack $\alpha = 40$ (deg), and a shallow flight path angle $\gamma = -0.85$ (deg) to avoid overheating. The dynamic pressure is only 4 (psf) and it is controlled using a combination of aero-surfaces and RCS jets for more effectiveness. The input file also includes a batch set for fast processing the data. The vehicle modeling program will process the vehicle data to create several state-space systems which are saved in file “Shuttle_Entry_RB.Qdr”. There is a system with title: “Shuttle Early Hypersonic Re-Entry, Rigid Stabil Axes Model for LQR” that will be used for control synthesis. This system is separated into pitch and lateral subsystems used in separate LQR designs. There are two additional vehicle data-sets created for calculating mixing-logic gain matrices, a set for calculating an aero-surfaces mixing-logic matrix, and a set for calculating the RCS jets mixing-logic matrix. The simulation model title is: “Shuttle Early Hypersonic Re-Entry, Rigid Body Axes Model for Simulation”. The rates in this system are defined in the body axes and the turn coordination flag is set to: “No Turn Coordination”, which means, that a body to stability transformation of the rates and the turn coordination logic must be

included in the simulation model. The systems and mixing-logic matrices are also converted to Matlab format for further analysis using Matlab.

1.2 Control Surfaces

Even though the Shuttle Orbiter has multiple aero-surfaces only the inboard elevons, outboard elevons, and the rudder are used for flight control during early reentry. The body-flap is not active in the control loop but it is used for trimming, balancing the pitch moment to achieve the required (α), and providing good elevon effectiveness. Its position is pre-scheduled and it also protects the main engines which are not active during reentry. There is also a split-rudder for speed-braking which is used only near landing and it will not be included in this model. The left and right outboard elevons are mainly used for roll control, the left and right inboard elevons are used mainly for pitch control, and the rudder is mainly for yaw control. But there is a significant amount of coupling between roll and yaw. The hinge vectors of the four elevons are almost horizontal along +y axis (slightly tilted because of the wing dihedral) and perpendicular to the vehicle x axis, $\lambda_{cs}=0$. The rudder hinge vector is rotated at $\phi_{cs}=90$ degrees about x, and it is not exactly vertical but it has a back-sweep of $\lambda_{cs}=20$ degrees from the z-y plane.

The exact combination of the aero-surfaces to achieve roll pitch and yaw control is dictated by the mixing logic matrix “KSmix”. This matrix translates the control demands into surface deflections. During early reentry the elevons in combination with the body-flap are commanded open-loop to trim the vehicle at 40 degrees of angle of attack. The surface deflections balance the pitching moment created by the $\alpha=40^\circ$. The elevons, however, also receive an additional feedback signal from flight control to maintain the proper vehicle attitude. The locations of the aero-surfaces, their mass properties, hinge orientation angles, hinge moment coefficients, and aerodynamic coefficients are defined in the input data-set.

1.3 Reaction Control System Thrusters

The Space Shuttle orbiter has three RCS modules, a forward module and two RCS pods in the rear (left and right). The vehicle has 38 primary reaction control jets plus vernier jets. However, in order to simplify the control design and analysis in the current model we have combined together the jets which are close together and are firing in the same directions into single thruster groups, capable of firing at multiple thrust levels. The simplified RCS model in the vehicle data file “*Shuttle_Entry_RB.Inp*”, consists of five thrusters in the front module and three thrusters per rear RCS pod. They are capable of thrusting in both positive and negative directions and at multiple thrust levels (defined as throttle levels). The three thrusters in the left rear pod are firing along $\pm Z$ and +Y, and the three thrusters in the right rear pod are firing along $\pm Z$ and -Y. In the front module we have two thrusters firing along $\pm Y$, one thrusting along +Z, and two skewed thrusters mainly along -Z. Each rear thruster physically represents a combination of three 800 pound jets that can produce a maximum of 2400 pounds of thrust in the specified direction. Each of the front thrusters physically represents a combination of two 800 pound jets that produces a maximum of 1600 pounds of thrust. Each thruster group is represented in the data by a single engine that is nominally at zero thrust, it does not gimbal, but it can vary its thrust between zero and \pm maximum thrust which is either ± 2400 or ± 1600 . Each thruster data include its location relative to vehicle coordinates, its maximum thrust, and the direction of firing defined by the pitch and yaw mounting angles (Dyn, Dzn).

When using the state-space model in a simulation the range of the throttle input for each thruster should vary between (0 to +1) for a single directional thruster or between (0 to ± 1) for a two

directional thruster. Negative throttle values indicate negative thrust or firing in the opposite direction. Throttle inputs greater than one mean that the engine must produce a thrust greater than what it is capable. A zero input means that thrust is zero and an input of (+1) means that the thrust is at its max level, which is either 2400 (lb) for a rear thruster or 1600 (lb) for a front thruster. Intermediate throttle inputs between zero and one are acceptable if the thrusters are producing a continuous thrust. In most cases, however, this is not acceptable because in general RCS jet thrusts are either zero or max thrust. In this case, however, we are allowing some thrust variation, or a thrust quantization rather, because we are allowing each jet in a thruster group to fire independently in the same direction, as needed, to produce a 2 or 3 level thrust control. We will introduce, therefore, a multi-level throttle control logic that generates throttle commands to the thrusters that include some intermediate values in addition to zero and one. The quantized commands to a 3-level rear thruster will be either {0, 1/3, 2/3, or 1} that corresponds to either zero, one, two, or three 800 (lb) jets firing from a single location and in the same direction. Similarly, the quantized inputs to one of the 2-level front thrusters can either be {0, 0.5, or 1} that corresponds to either zero, one or two 800 (lb) jets firing in the same group. The flight control logic determines the number of jets to be fired at each thruster location according to the amount of attitude error in both magnitude and direction.

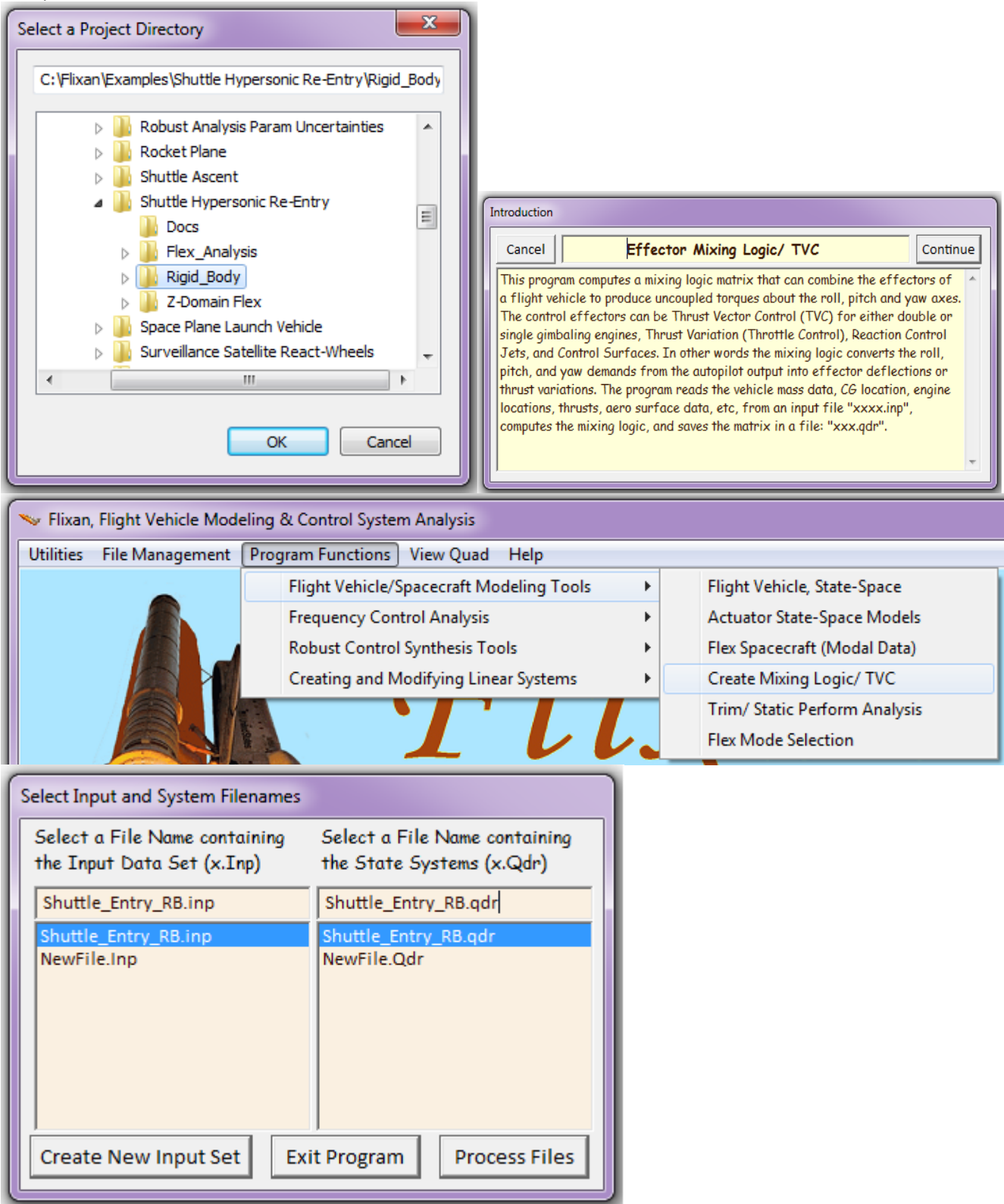
1.4 Mixing Logic Matrix

The mixing logic matrix converts the roll, pitch, and yaw acceleration demands coming from the flight control system to effector commands, that is, surface deflections or throttle commands. Since the vehicle in this flight condition is controlled by two separate aero-surfaces and RCS control systems we will design two mixing logic matrices: a matrix “KSmix” that converts the surfaces flight control system outputs to deflections for the five surfaces, and a matrix “KJmix” that converts the RCS flight control outputs to 11 throttle commands. The two mixing logic matrices are derived independently from each other. In addition to roll, pitch, and yaw acceleration inputs the KJmix thruster mixing matrix has a fourth input to accommodate a normal acceleration demand from the flight control system. The (11x4) KJmix matrix has four inputs and 11 outputs that can throttle the eleven thrusters in multiple levels and capable to control the vehicle in four independent directions: three rotational plus Nz acceleration. The Nz degree-of-freedom in the KJmix matrix is needed in order to provide attenuation in the phugoid resonance by applying Nz-feedback via the RCS thrusters.

The mixing logic matrices are derived by using the mixing logic utility program in Flixan. The program reads the vehicle and effector data set from the input data file and calculates the mixing logic matrix, which is the pseudo-inverse of the vehicle model. It converts the desired accelerations into surface deflections or throttle commands. The input data file “*Shuttle_Entry_RB.inp*” includes two additional vehicle data-sets which are not intended to generate vehicle models but to be used by the mixing logic program and to create the mixing logic matrices: KSmix and KJmix. The title of the third vehicle data-set used to create the aero-surfaces mixing matrix KSmix is “*Shuttle During Early Hypersonic Re-Entry, for Surface Mixing Logic*”. It includes the five aero-surfaces but not the RCS jets. The title of the fourth vehicle data set used to create the RCS mixing matrix KJmix is “*Shuttle During Early Hypersonic Re-Entry, For Jet Mix Logic*”. It includes the 11 RCS thrusters but the aero-surfaces are removed.

Let us now use the mixing logic program interactively to generate the thruster combination matrix KJmix. Start the Flixan program and go to directory “*C:\Flixan\Examples\Shuttle Hypersonic Re-Entry\Rigid_Body*”. From the main menu go to “*Program Functions*”, “*Flight Vehicle/ Spacecraft Modeling Tools*”, and then select “*Create Mixing Logic/ TVC*”, as shown below. From the filename

selection menu select the input data file “*Shuttle_Entry_RB.inp*”, the output systems file “*Shuttle-Entry-RB.Qdr*”, and click on “*Process Files*”.



From the following vehicle data selection menu select the title “*Shuttle During Early Hypersonic Re-Entry, For Jet Mix Logic*” that contains only the RCS jets, and click on “*Run Input Set*”. The next

back a combination of states, mostly angle of attack and integral of angle of attack, but also pitch rate and small amounts of attitude feedback and normal acceleration. The lateral control system uses also state-feedback consisting of roll and yaw rates measured in stability axes, angle of sideslip (β), β -integral, and integral of roll rate.

The control system during early reentry uses a blended combination of aero-surfaces and RCS jets in parallel, for both pitch and lateral directions. The control surfaces are not very effective because of low dynamic pressure. The RCS is a lot more effective but expensive because it requires fuel. Under normal quiescent conditions when the disturbances and command variations are small the control surfaces are sufficient to maintain a low bandwidth stabilization without firing the jets. The aero-surfaces control system is capable to trim and stabilize the vehicle as long as the disturbances are small. The RCS control is present in parallel to further enhance the system performance. It is activated when additional power is required, either in the beginning of a maneuver to accelerate the vehicle response or to react against an unexpected disturbance. When the control errors are small the RCS controller is not active and the position is maintained by the aero-surfaces system.

Pitch Control System

The pitch control system presented in this analysis was designed using the pitch plant model “*Shuttle Hypersonic Re-Entry, Rigid Stabil Axes Model for LQR, Pitch Axis-2*”. This system was extracted from the coupled stability axes model, as already described, and it includes the mixing logic matrices for both: RCS and aero-surfaces. It was exported to the Matlab analysis directory as system function “*veh_i_pdes2.m*”. Only the pitch states, inputs and outputs were retained in this reduced model. With the mixing logic matrices included, the pitch design model has three inputs: a pitch control input (q -dot) and Nz acceleration commands associated with the RCS control loop, and one pitch control input (q -dot) associated with the aero-surfaces control loop. The pitch control system simulation model with the two state-feedback loops closed is in file “*Sim_Pitch.mdl*” and it is shown in Figure (3). An alpha-integral state is also included in the design model to improve alpha tracking. The control system was designed in two steps: (a) the low-bandwidth aero-surface control system is designed first to stabilize the vehicle using only the four elevons, with the RCS loops opened, and (b) with the aero-surfaces loop closed, a second (parallel) state-feedback loop is designed using the two (q -dot and Nz acceleration) RCS inputs to further enhance the system bandwidth and performance.

The two state-feedback controllers are shown operating in parallel in Figure (3). The aero-surface controller is a four-state-feedback row vector that closes the loop between the states and the elevon input. The RCS controller is a (2x4) state-feedback gain matrix (K_{pr}) that closes the loop between the states and the two RCS input demands, pitch and Nz acceleration demands. The system is designed to maintain stability with either loop opened, since the RCS is not always active, and the aero-surfaces effectiveness may sometimes not be sufficient for maneuvering. Note, that in this simple model the actual vehicle effectors are not visible because they are “hidden” inside the plant model. Only the inputs to the effector combination matrices are visible. Also, we are assuming that the thrusters are providing a continuous (analog) thrust and that the thrust is allowed to assume positive and negative values. This is obviously not accurate and the controller needs to be further modified in our future versions in order to represent reality.

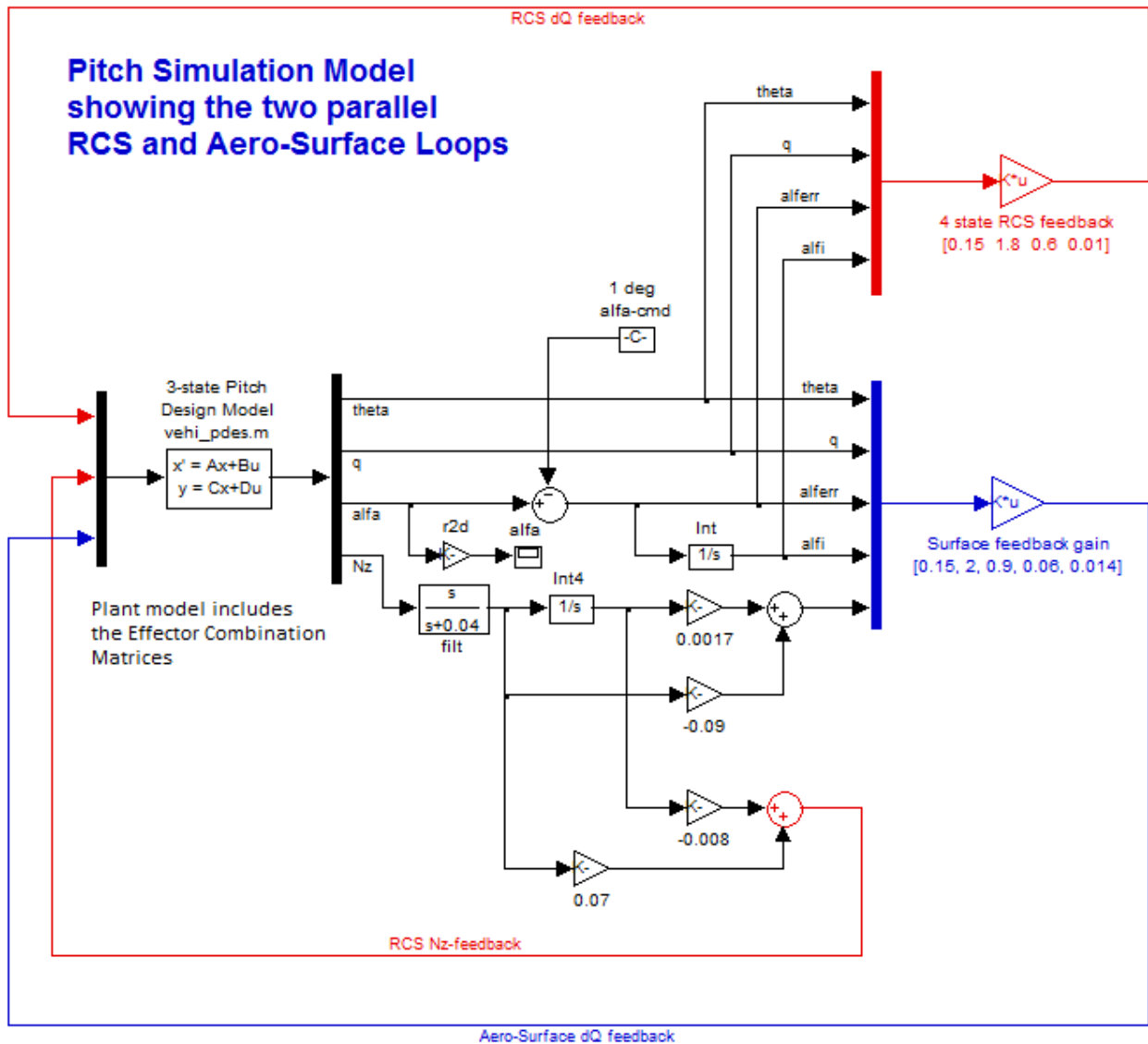


Figure (3) Pitch state-feedback control system showing a control surfaces loop and a linear RCS loop in parallel

Lateral Control System

In the lateral directions the roll and yaw coupling is very strong and the LQR method can be very effective in designing a stabilizing state-feedback law. The lateral system “*Shuttle Hypersonic Re-Entry, Rigid Stabil Axes Model for LQR, Lateral Axes*” was used as a design plant. This system was extracted from the coupled stability axes model and it includes the mixing logic matrices for both, RCS and aero-surfaces as already described. It was exported to the Matlab analysis directory as m-file function “*veh_i_ldes.m*”. With the mixing logic matrices included in the model our design plant has four inputs: a pair of roll and yaw acceleration demands for the RCS loop, and a pair of roll and yaw acceleration demands for the aero-surfaces loop. The two control loops are designed separately. Note, that although the roll and yaw rate outputs in the lateral design plant “*veh_i_ldes.m*” obtained from the vehicle modeling program are defined in stability axes, the p and r states, however, were not converted and they are still in the body axes. That’s why the C matrix is not diagonal and the design system’s states must also be transformed to stability axes before we apply the LQR algorithm in this system.

This simple transformation is performed in the Matlab initialization file “run.m” and the lateral design system is transformed to define both: states and outputs in the stability axes prior to LQR. As we already discussed, the stability axes lateral plant is used instead a body axes system for control design because the vehicle is commanded to roll about the velocity vector and not the body x-axis.

```

% File run.m
d2r=pi/180; r2d=180/pi;
[Avp, Bvp, Cvp, Dvp]= vehi_pdes;           % Load Pitch Design Model
[Avl, Bvl, Cvl, Dvl]= vehi_ldes;          % Load Lateral Design Model
[A6d, B6d, C6d, D6d]= vehi_6dof;         % Coupled Body Axes Vehicle
load KSmix.mat -ascii;                    % Load Surfaces Mix Logic
load KJmix.mat -ascii;                    % Load RCS Jets Mix Logic

alfa0=40; VO=18640; Thet0=39.15;          % Additional Vehicle Parameters
calfa=cos(alfa0*d2r); salfa=sin(alfa0*d2r);

% Two Steps Lateral Control Design ....
Alv= Cvl*Avl*inv(Cvl); Blv= Cvl*Bvl;      % Convert State Vector to ...
[n,n]= size(Cvl); Clv=eye(n); Dlv=Dvl;    % Stability Axes, Outp=States

% Step-1, Using Only Aero-Surfaces
[Ap3,Bp3,Cp3,Dp3]= linmod('Ldes5x');      % 5-state model {p,r,bet,pint,betint}
R=[1,25]*2; R=diag(R);                    % CS LQR Weights R=[1,10]*2
Q=[1 1 1 0.05 0.05]*0.8; Q=diag(Q);      % CS LQR Weights Q=[1 1 1 0.04 0.04]*0.4
kls=lqr(Ap3,Bp3,Q,R); acl=Ap3-Bp3*kls; eig(acl) % Perform LQR design on control surfaces

% Step-2, Using RCS Jets (With Aero-Surfaces Loop Closed)
[Ap4,Bp4,Cp4,Dp4]= linmod('LCS_Closed');  % RCS des model/ Surfaces Loop Closed
R=[1,5]*0.2; R=diag(R);                    % CS LQR Weights R=[1,5]*0.2
Q=[1 1 1 0.2 0.05]*0.4; Q=diag(Q);        % LQR Weights Q=[1 1 1 0.2 0.05]*0.4
klr=lqr(Ap4,Bp4,Q,R); acl=Ap4-Bp4*klr; eig(acl) % Perform LQR design on the RCS

label='Yaw Axis Aerosurface Loop Stability (RCS opened)';
[As,Bs,Cs,Ds]= linmod('Anal_6dof');        % Frequ Response Model
sys=ss(As,Bs,Cs,Ds);                       % Perform Linearization
w=logspace(-3,3.5,8000);                    % and Frequ domain analysis
figure(1); Nichols(sys,w); title(label)
figure(2); Nyquist(sys,w); title(label)

```

One additional modification is needed in the lateral design plant to enhance maneuvering performance before it can be used in LQR control synthesis. In addition to p_stab, r_stab, and beta, the state vector is augmented by introducing two additional states, the integral of roll rate about the velocity vector (p-stability-integral) for better tracking of the roll command, and beta-integral for further minimizing the steady-state side loads on the vehicle. The lateral control design is accomplished by file "run.m" in two steps:

1. In the first step a stabilizing low-bandwidth lateral control system is designed using the aero-surfaces loop only. It uses the aero-surface roll and yaw input demands p-dot and r-dot, with the RCS loops opened. The design plant is "Ldes5x.Mdl" shown in Figure (4).
2. In the second step the design plant has aero-surface loops closed, and a parallel RCS state-feedback loop is designed using the RCS roll and yaw input demands p-dot and r-dot to further enhance the system bandwidth and performance. The design plant is "LCS_Closed.Mdl" shown in Figure (5). The combined lateral control system is shown closed-loop in Figure (6).

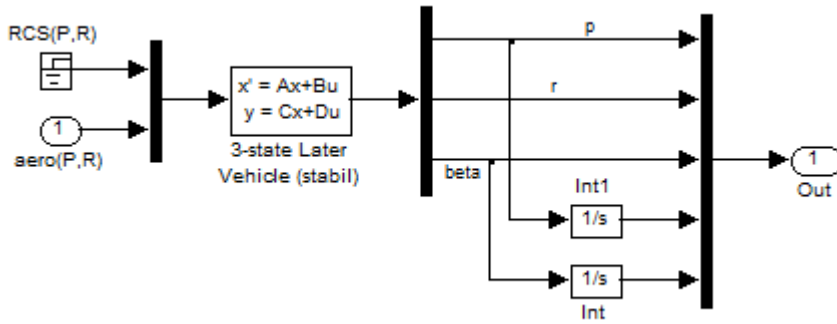


Figure (4) 5-state Lateral LQR Design Plant for Aero-Surfaces Only, in file "Ldes5x.Mdl" (RCS Not Used)

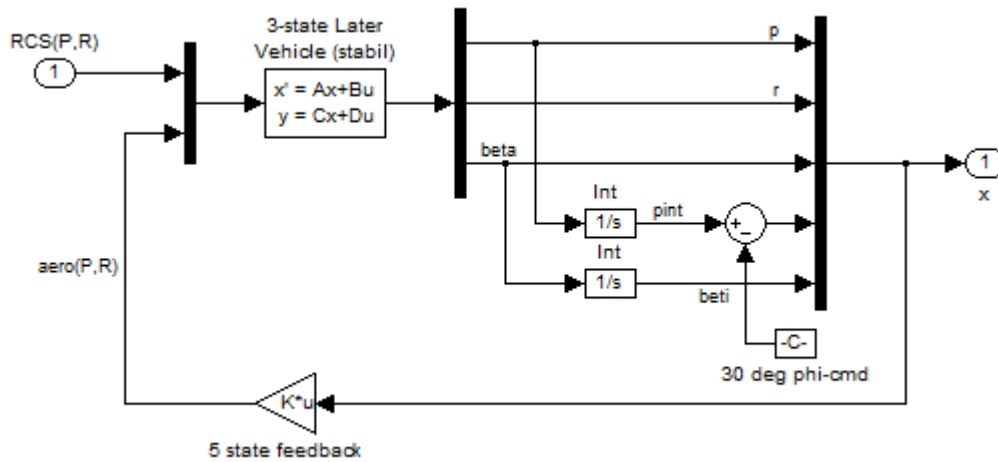


Figure (5) 5-state Lateral LQR Design Plant for RCS Control, in file "LCS_Closed.Mdl" (Aero-Surfaces Loop is Closed)

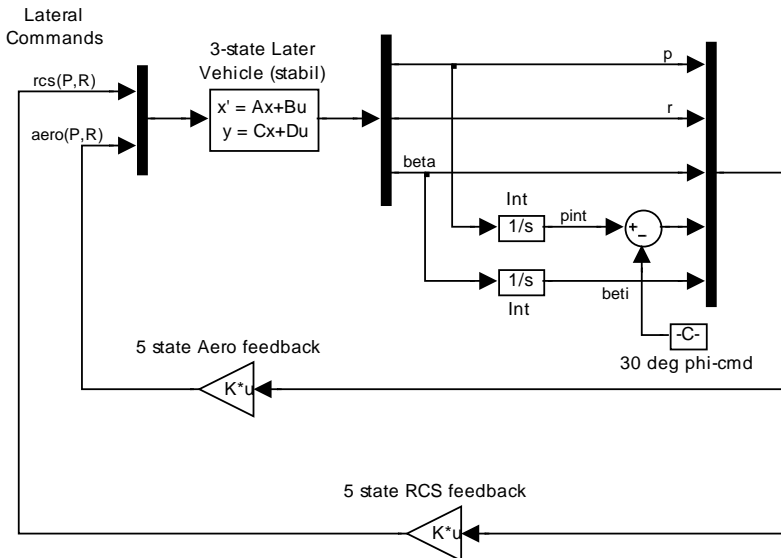


Figure (6) Lateral state-feedback control system showing the two loops Aero and RCS in parallel

It consists of two state-feedback controllers, similar to the pitch axis: a (2x5) aero-surfaces state-feedback gain matrix (K_{Is}) that closes the loop between the states and roll/ yaw p-dot and r-dot aero-surfaces demands, and a (2x5) RCS state-feedback gain matrix (K_{Ir}) that closes the loop between the states and the roll/ yaw p-dot and r-dot RCS demands. The system is designed to maintain stability using aero surfaces alone without RCS. The RCS system will be further upgraded in a more refined 6-dof simulation with a more realistic representation of the thruster firing, an improved switching logic to provide positive throttling and at discrete firing levels between zero and one. In a time-varying 6-dof simulation the flight control system gains are derived at fixed flight conditions, at selected Mach numbers, angles of attack, and dynamic pressures that cover a wide range of flight conditions. The control gains are tabulated as a function of Mach, alpha, and q-bar, and they are interpolated using look-up table logic.

1.7 Six-Dof Simulation Models

The vehicle state-space system that will be used to create this upgraded 6-dof simulation is: “*Shuttle Early Hypersonic Re-Entry, Rigid Body Axes Model for Simulation*”. It was created from file “*Shuttle_Entry_RB.Inp*” and it was saved in file “*Shuttle_Entry_RB.Qdr*” and also as a separate system function in file “*Vehicle_6dof.m*” which is loaded by the initialization file “*run.m*” and analyzed in Matlab. Its outputs rates are defined in the body axes and the turn coordination flag is set to “*No Turn Coordination*” which means that in order to use the body rates they must be converted to stability rates and the turn-coordination cross-feed must be included in the model.

1.7.1 Preliminary Simulation Model

A preliminary simulation of the coupled pitch and lateral system is implemented in the Simulink model in file “*Sim-6Dof-cont.Mdl*”, shown in Figure (5). The discrete jet firing has not yet been implemented and it assumes that the thrusters produce analog thrusts proportional to the error signal. This model is used as an intermediate step to evaluate the system performance and to adjust the design with both loops: the aero-surfaces and the analog thrusters working in parallel. This Simulink model uses the vehicle state-space system “*Shuttle Early Hypersonic Re-Entry, Rigid Body Axes Model for Simulation*” that was exported as a Matlab function “*vehi_6dof.m*”. Its output rates are in the body axes and the turn-coordination dynamics are not included because these functions belong in the control law.

6-dof Rigid Body Simulation Model Using Analog Jets

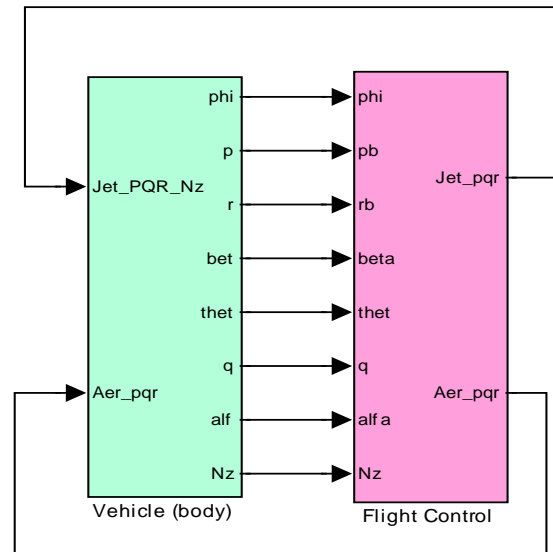
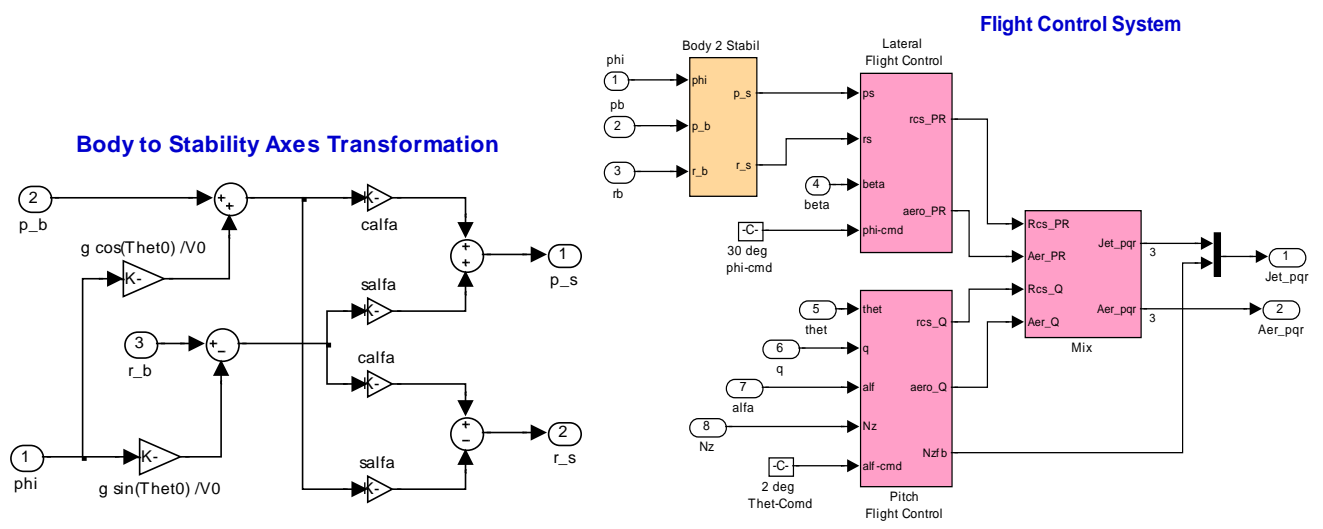
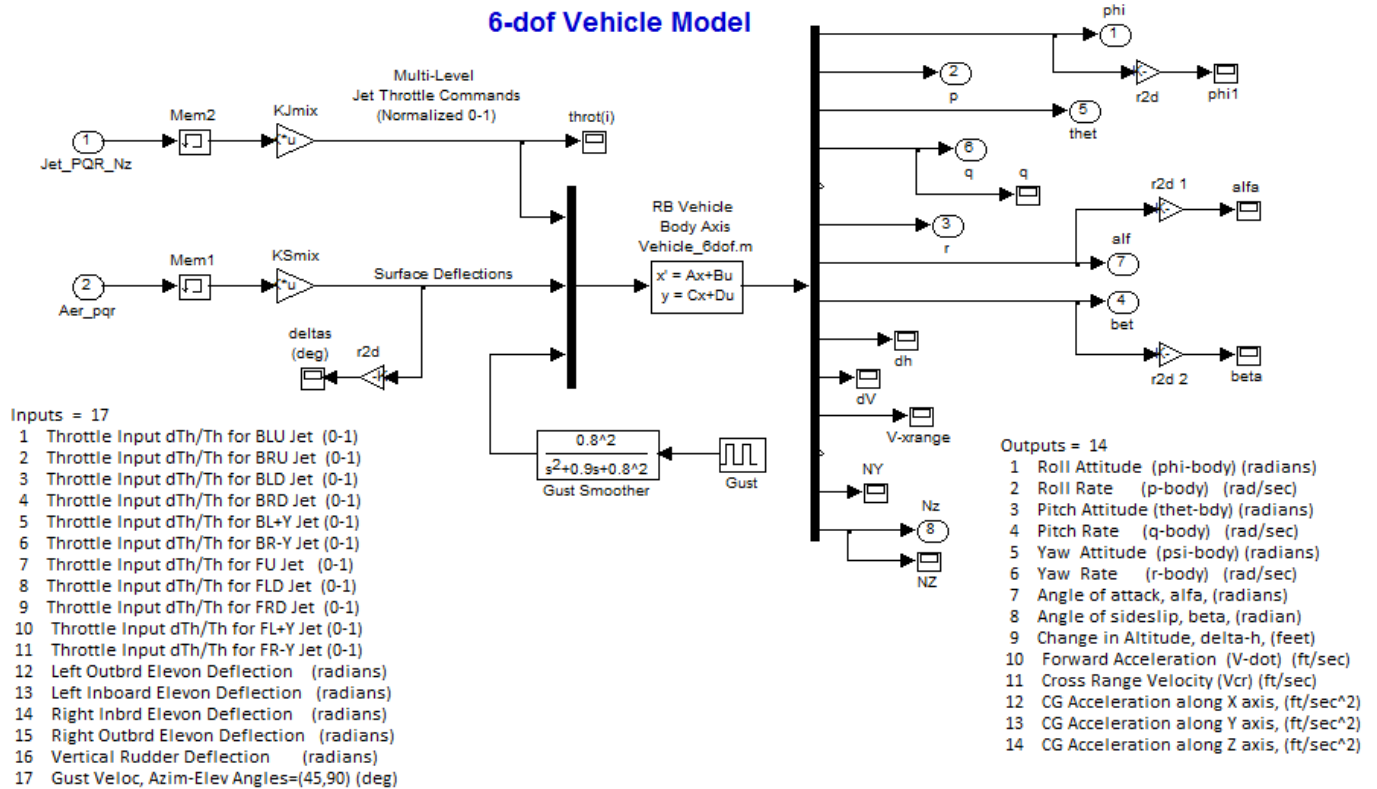


Figure (5a) shows the vehicle block in detail. In the center it contains the vehicle system. The RCS mixing matrix KJ_{mix} converts the 4-input flight control demands to 11 linear throttle commands. Similarly, the mixing matrix KS_{mix} converts the 3-input flight control demands in 5 aero-surface deflections. A smoothed gust velocity disturbance is applied to input 17 to analyze the vehicle response to gusts. The flight control system is shown in figure (5b). It consists of both pitch and lateral control laws and their outputs are combined into vectors, a four-commands vector: roll, pitch, yaw, and Nz acceleration demands for the RCS loop, and a three-commands vector: roll, pitch, yaw acceleration

demands for the aero-surfaces loop. In the lateral system there is a transformation block that converts the roll and yaw rates from body to stability axes. It also adds the linearized turn-coordination terms. Remember? It was included in the lateral design model by setting the flag “Include Turn Coordination”. The LQR derived state-feedback controller assumes that there is turn-coordination logic in the software. So it must also be included in this model. The pitch rate does not need transformation because it is the same in both body and stability axis.



1.7.2 Pulse-Width Modulation and Multi-Level Thrusting

In the previous sections we have been gradually building up our simulation models for the purpose of eventually coming up with a more realistic implementation of the RCS jets operating in parallel with the aero-surfaces. In our previous simulation we assumed that the RCS thrusters are producing a variable and continuous thrust and that the thrust is can also be negative. This is far from reality. We must now modify our jet firing system with something equivalent that preserves the basic RCS design concept, but also practically realizable. The first problem to be fixed is the negative thrusting issue. Each thruster is receiving a signal from flight control via the KJmix matrix and this signal may be positive or negative based on the direction of the error vector signal. It seems feasible because of the multiplicity of thrusters and their placement symmetry, that it is possible to zero out all the negative throttle commands (created by the current logic) and compensate by doubling the throttle commands on the thrusters that receive positive commands, without introducing a significant amount of error towards achieving the corrective action. This takes care of the negative thrusting problem.

The second problem that needs to be fixed is the analog thrusting. We know that an RCS jet cannot produce a variable thrust. It is either off or at maximum thrust. In this case, however, we do have the luxury of combining two or three jets per thruster location which permits multi-level thrusting in multiples of 800 (lb), two levels thrusting in the front module and three levels thrusting in the rear RCS pods. But even a multi-level thruster mechanization is not nearly as efficient as the original continuous thruster design and the LQR design which was based on continuous operation might still fail when discretizing the thrust. One idea that preserves the original LQR thruster control design is to implement a thruster firing cycle that modulates the thruster firings sufficiently fast, relative to the system bandwidth, as to produce an average thrust that is equivalent to the commanded analog thrust.

This firing sequence can be achieved by using a PW modulator. Each thruster combination (2 or 3 jets) has a control logic that regulates both the thrusting level and the PW modulation of each jet. The PW modulation and the multi-level functions are working together in a superposition fashion. The input to the modulator is the throttle command that varies between zero and +1. The output is a PW modulated square wave with an "on" and "off" time ratio that is a function of the throttle command.

Figure (6a) shows a PW modulator for a single thruster receiving a throttle command input between zero and +1. In the example shown in figure (6b) below, we apply a sinusoidal signal to the modulator that cycles between zero and +1. The output is a PW modulated signal that produces a square signal that switches between {0, and +1}. The average value of the output signal over a short period is always positive and approximately proportional to the magnitude of the input throttle command signal. When the input signal is small in amplitude (less than 0.1) the average output is mostly zero. As the input signal magnitude increases the average "on" versus "off" ratios between 0 and +1 increases, and when the input is close to +1, the +1 time intervals in the PW modulated square wave output are much longer in comparison with the zero intervals. The PW modulator concept presented here is mainly for simulation purposes. An actual hardware design of multiple thrusters operating in PW modulation mode is a more complex issue and beyond the scope of this example, especially when one has to consider thruster failures and redundancy management.

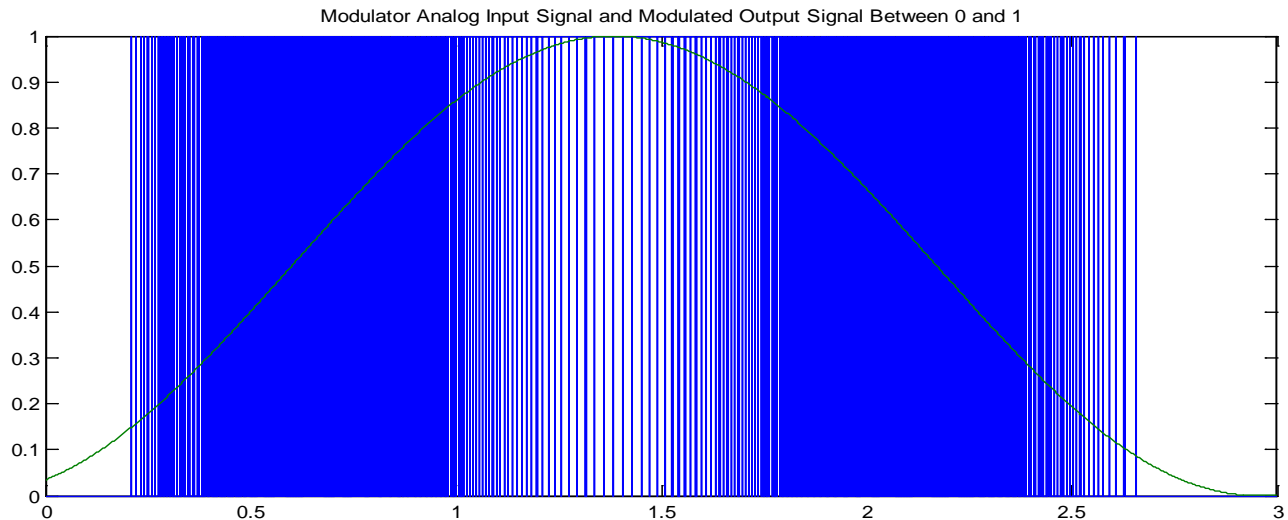
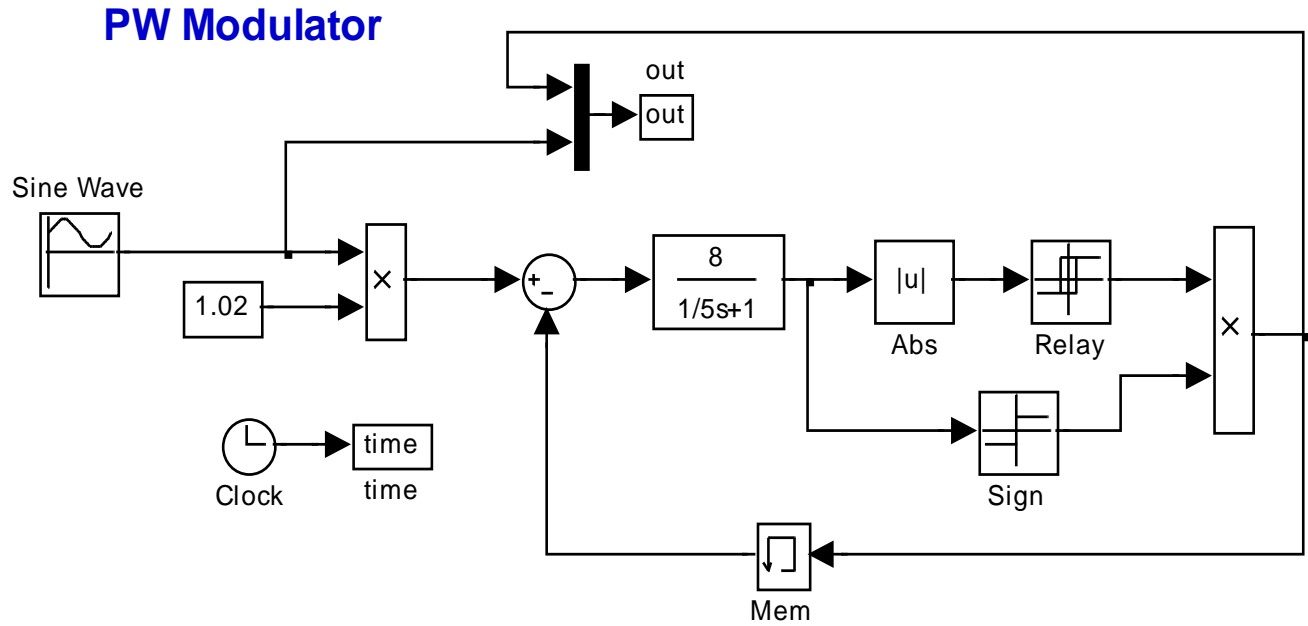


Figure (7) PW Modulator produces an average thrust that is proportional to the commanded thrust. In this case it represents the throttle commands that varies between (0 and +1).

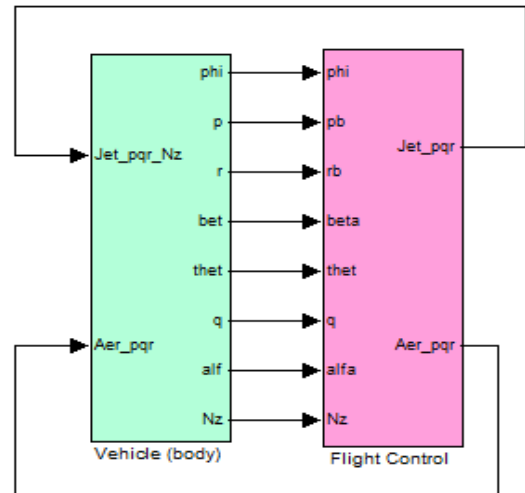
By combining two or three modulators together, depending on the number of independently firing jets per cluster, we can implement a multilevel throttling capability between zero and one (either in 2 levels for the front thrusters or in 3 levels for the rear thrusters). Zero indicates no firing, and one indicates maximum thruster firing. In our example we have 11 multi-level firing thrusters, an input of +1 in one of the rear thrusters signifies that all three jets in the same location are firing together in the same direction to produce a total 2400 (lb) of force.

1.7.3 Simulation Model using the Multi-Level Thrusters and Pulse-Width-Modulators

Figure (8) shows a 6-dof Simulink model “*Sim-6Dof-pwm.mdl*” that is similar to the one described in section (1.7.1) with the exception that the continuous thrusters are replaced with the PWM thruster firing logic. The vehicle dynamics (green) subsystem is shown in detail in Figure (8.a). The vehicle state-space system is: “*Shuttle Early Hypersonic Re-Entry, Rigid Body Axes Model for Simulation*” that is loaded from file “*Vehicle_6dof.m*”. The last input is a filtered wind gust.

The thruster firing logic is shown in detail in Figure (8.b). Each thruster uses a PW modulator similar to the one shown in Figure (7). The multi-level firing logic is implemented as a Matlab function “*Pos_Thrust3.m*”. The roll, pitch, yaw, and Nz acceleration demands are converted to PW modulated and multi-level throttle commands driving the thrusters. The matrix KJ_{mix} is still used inside the jet-selection function but the outputs are modified to produce positive throttle signals. In addition to multi-level thrusting this jet firing function disables the RCS operation when the magnitude of the flight control error becomes sufficiently small to allow the less costly aero-surfaces to complete the maneuver and to maintain stability. Thruster delays and minimum-on-time details are not included in the simulation.

6-dof Rigid Body Simulation Model Using PWM RCS Jets



Simulation Results

We will now use this latest Simulink model "*Sim_6Dof_pwm.Mdl*" to simulate the orbiter response to simultaneous commands of: 1 deg step in pitch, and 40 degrees step in roll about the velocity vector, and also a 50 (ft/sec) filtered wind-gust pulse. The direction of the gust is perpendicular the vehicle x-axis and at 45 degrees between the +z and the +y axes, as defined in the vehicle input data. After running the simulation, the file "pl.m" is used to plot the results as shown below.

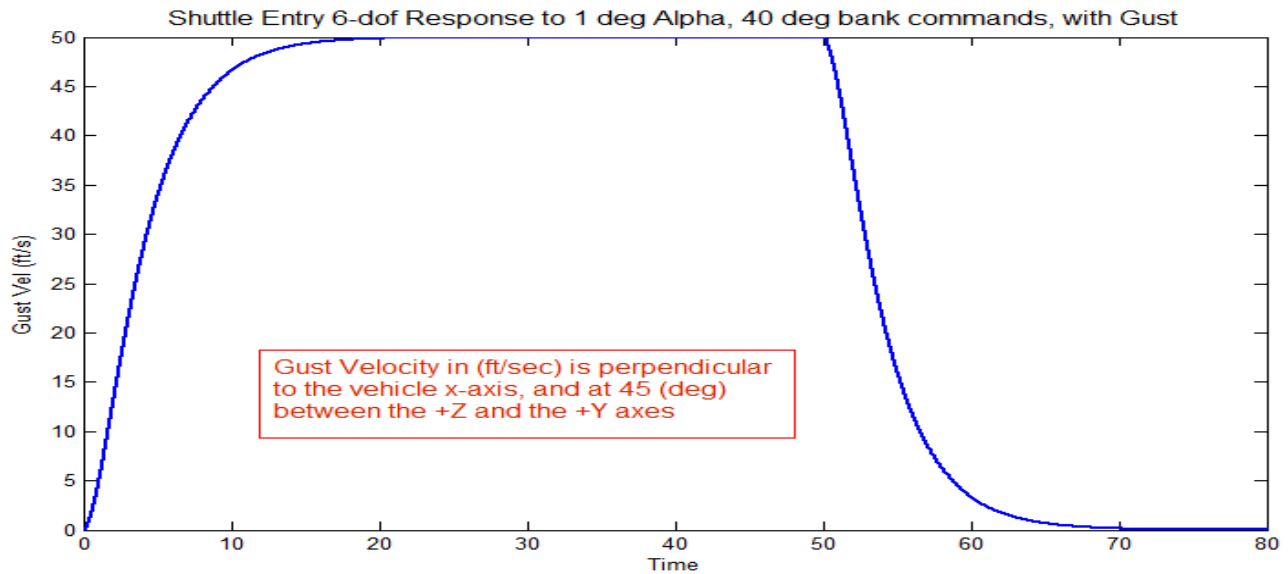


Figure (9a). The wind gust pulse was smoothed by a low-pass filter.

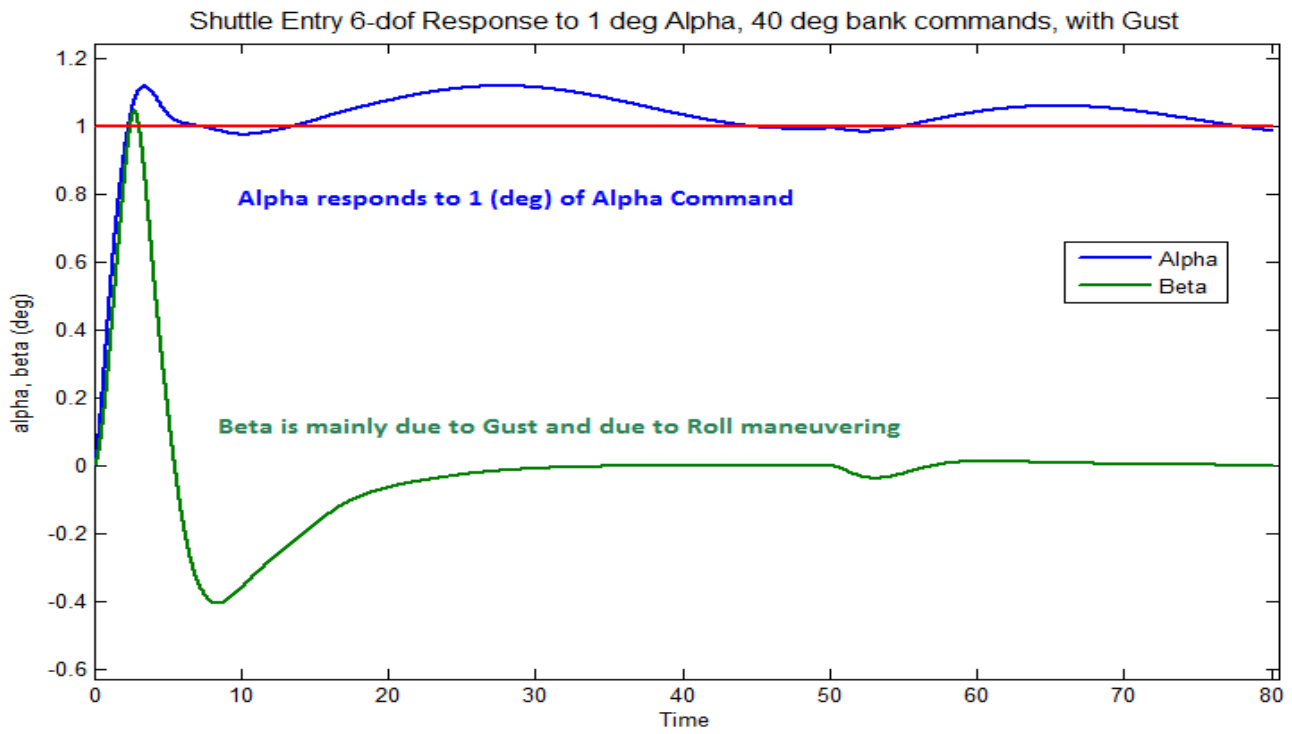


Figure (9b) The vehicle responds fast to the 1 deg of alpha command. The small low frequency oscillation on the top of alpha is caused by the lightly damped phugoid mode. The beta response is mainly due to gust and due to the roll maneuver.

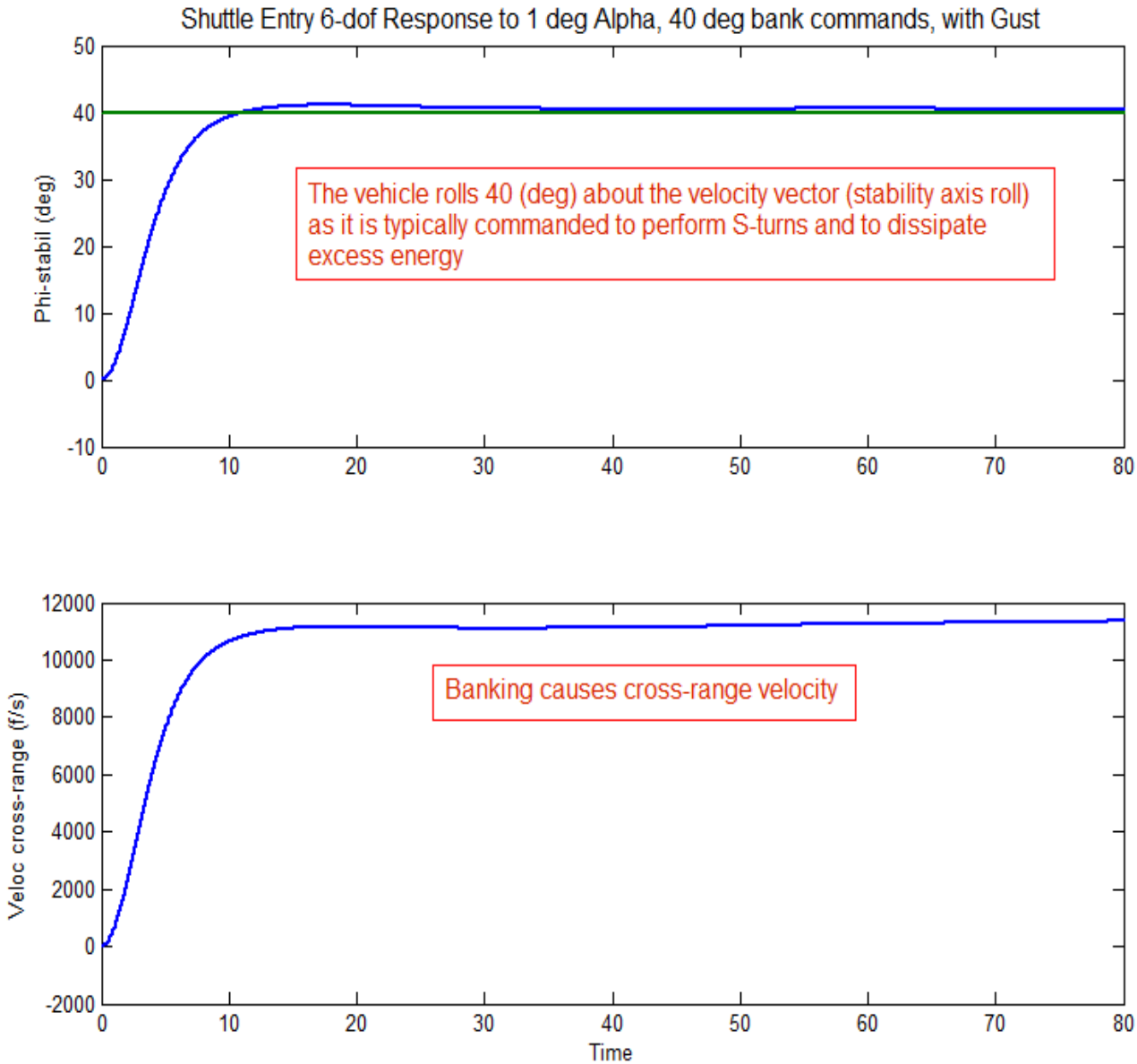


Figure (9c) shows the response to the 40 degrees roll-step command about the velocity vector. It takes 10 seconds to complete it with zero steady-state error because of the p-integral feedback. Banking also causes a cross-range velocity. It is used by closed-loop guidance to control the cross-range errors and also to perform S-turns to dissipate excess kinetic energy.

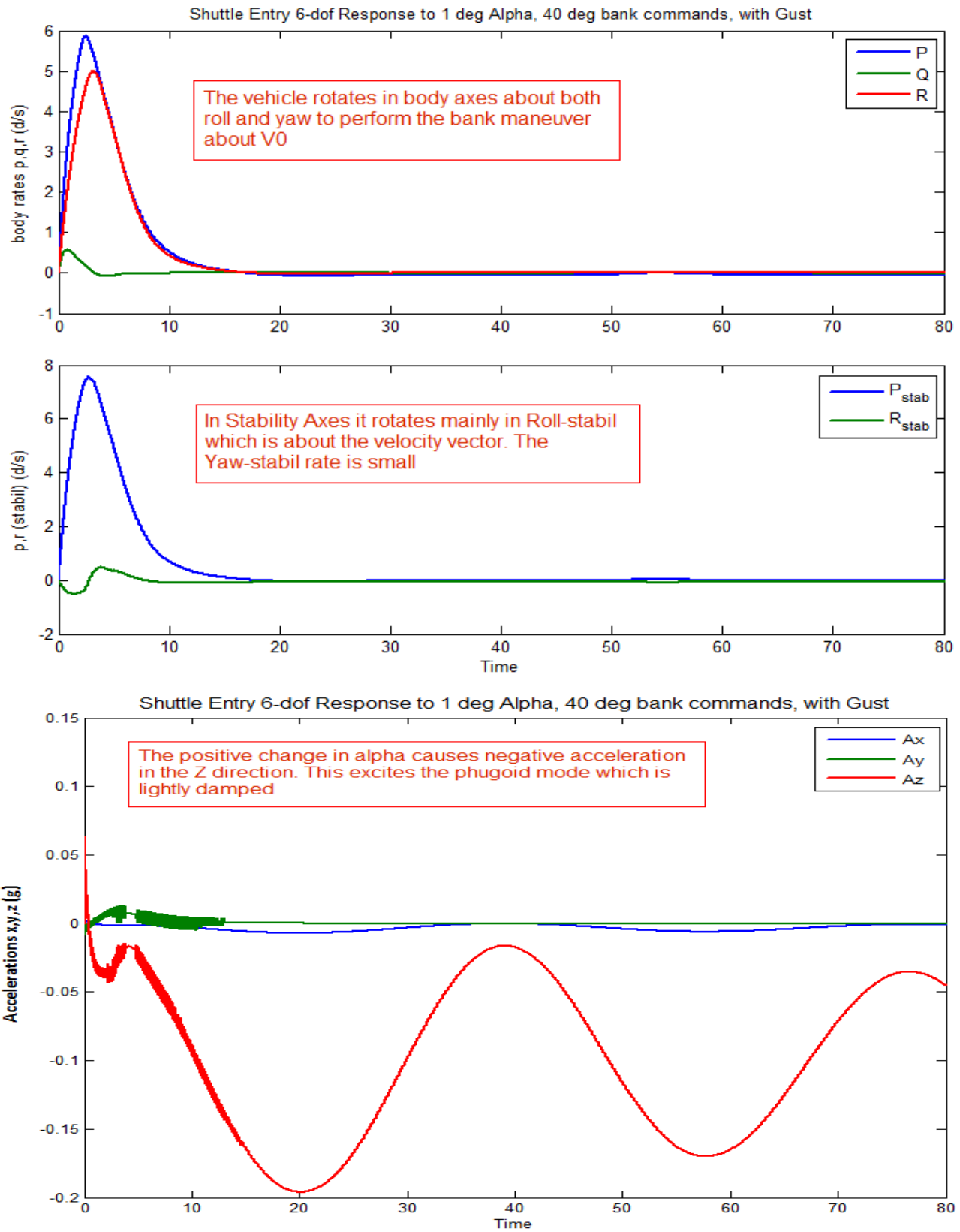


Figure (9d). The top plot shows the vehicle rates measured by the rate gyros in the body axes. The roll and yaw body rates are similar because the vehicle rotates simultaneously in both roll and yaw during the roll maneuver. The middle plot shows the roll and yaw rates in stability axes. Notice the big

difference in magnitude between the two rates because the vehicle rotates mainly about V_0 (stability roll) during the maneuver. The yaw rate is a transient mostly due to gust. In the bottom plot we see the effects of the gust and the pitch up maneuver that cause a negative N_z acceleration (up). This excites the phugoid mode which is lightly damped by the N_z -accelerometer feedback.

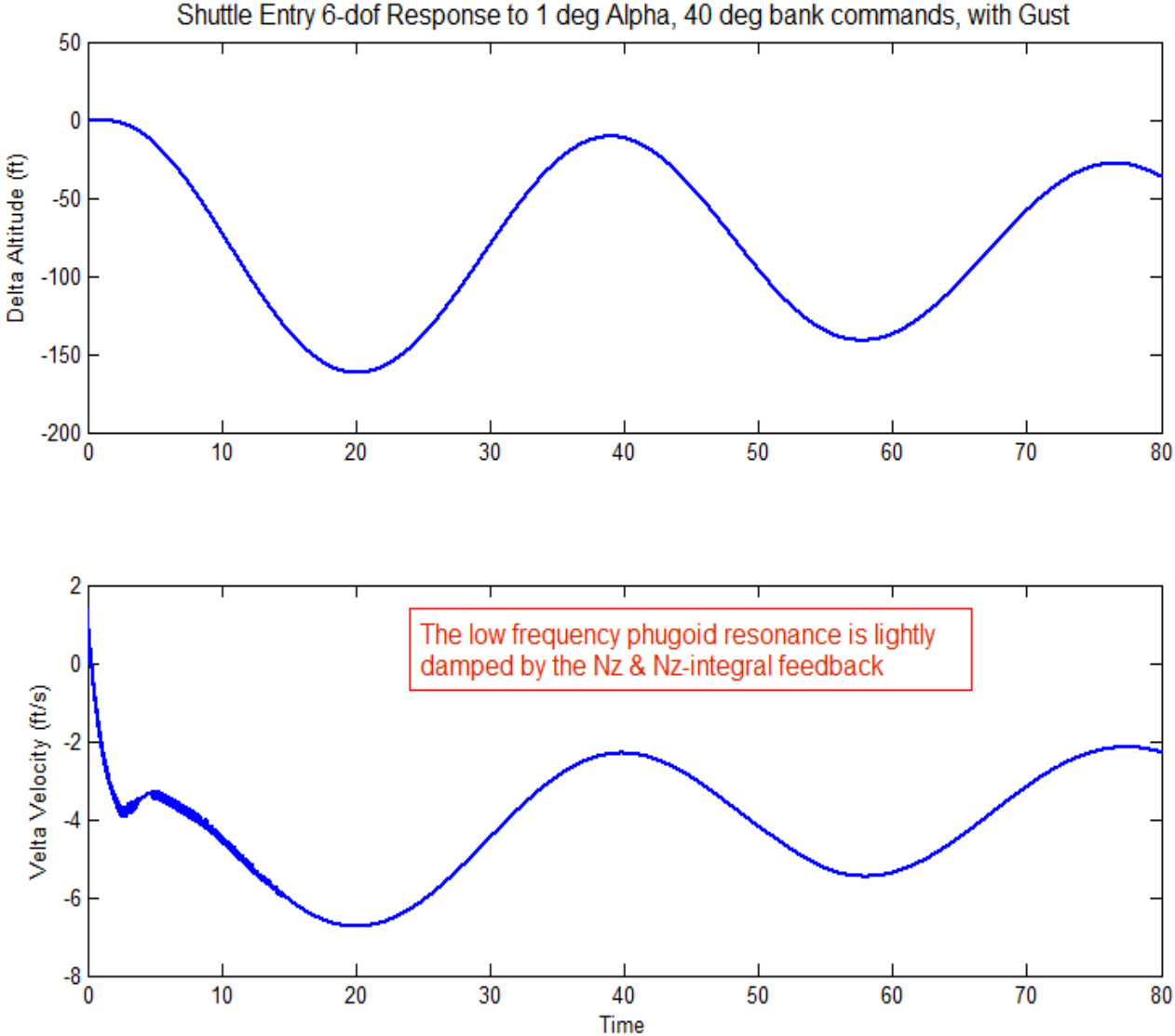


Figure (9e). The maneuver excites the phugoid mode which is lightly damped as shown by the variations in altitude and velocity plots. N_z and N_z -integral feedback is used to lightly dampen the phugoid mode.

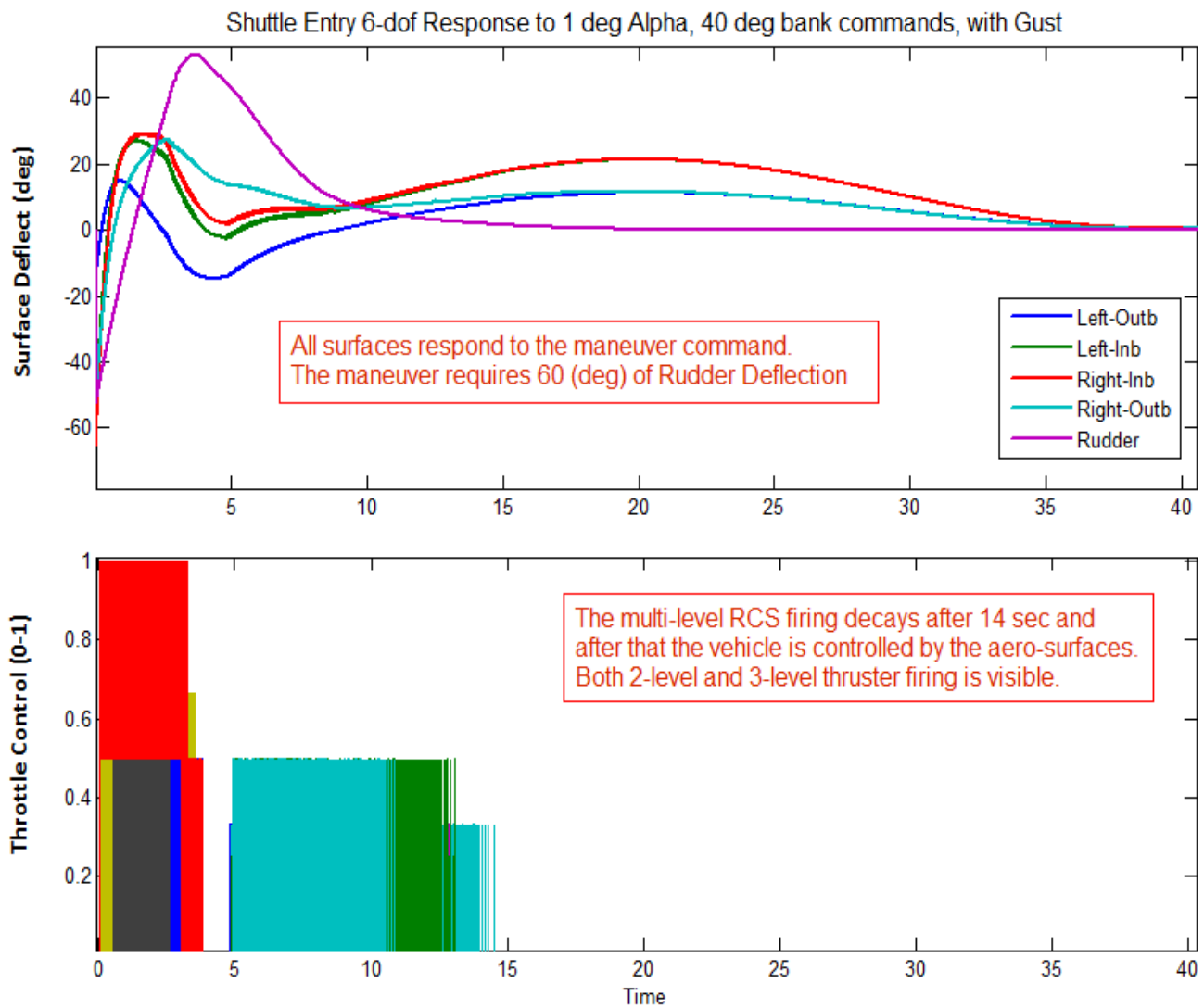
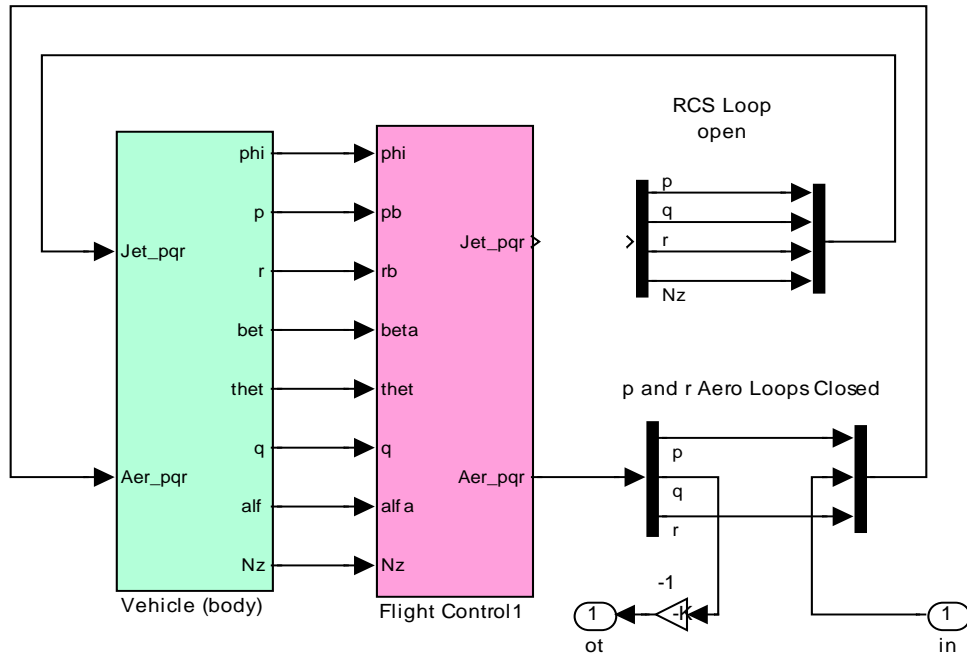


Figure (9f) shows the control activity in the aero-surfaces and RCS thrusters. The top plot shows the 5 aero-surface deflections, and the bottom plot shows the throttling of the 11 multi-level RCS thrusters which is regulated by the firing logic between (0 and +1). All surfaces contribute to the maneuver. The initial rudder deflection is significantly large because of the size of the roll maneuver. Later on the elevons oscillate as they respond to the phugoid mode. Initially, the RCS activity is strong during the first 14 sec because it is needed to execute the maneuver. Later, when the control error is reduced the RCS is turned off.

1.8 Linear Stability Analysis

The Simulink model “*Anal_6Dof.mdl*” in Figure (10) is used to perform linear stability analysis in the frequency domain. It consists of the same vehicle and flight control element blocks as in the simulation model described in section (1.7.1), using continuous RCS thrusters.

6-dof Rigid Body Analysis Model



Pitch Aero Loop Stability Analysis

Figure (11) Linear frequency response model for stability analysis

On the right side, the RCS and the aero-surface loops are expanded from vectors and they can manually be wired by opening and closing the proper loops for frequency response analysis one loop at a time. The aero-surfaces control system consists of three (roll, pitch, yaw) loops. The RCS consists of four loops (p, q, r, and Nz) control. The Simulink model can be modified by closing and opening the various loops as needed based on the loop to be analyzed. For example, in order to check the pitch axis stability using aero-surfaces alone, we open all RCS loops because we want to analyze the aero-surfaces system by itself, close the roll and yaw aero-surface loops and calculate the frequency response across the open pitch loop, as shown in the Nichols chart in Figure (12). The aero-surfaces system must have sufficient stability not only when both control systems are operating together, but also when the RCS is "off". The file “run.m” performs the frequency response analysis. It creates a SISO system of the user modified model “*Anal_6Dof.mdl*” and calculates the frequency response across the two opened ends.

Figure (13) shows the Simulink model “*Anal_6Dof.mdl*” modified to analyze the RCS loop stability in pitch with the aero-surface loops closed. The RCS roll, yaw, and Nz loops are also closed and the frequency response is calculated across the opened pitch RCS loop.

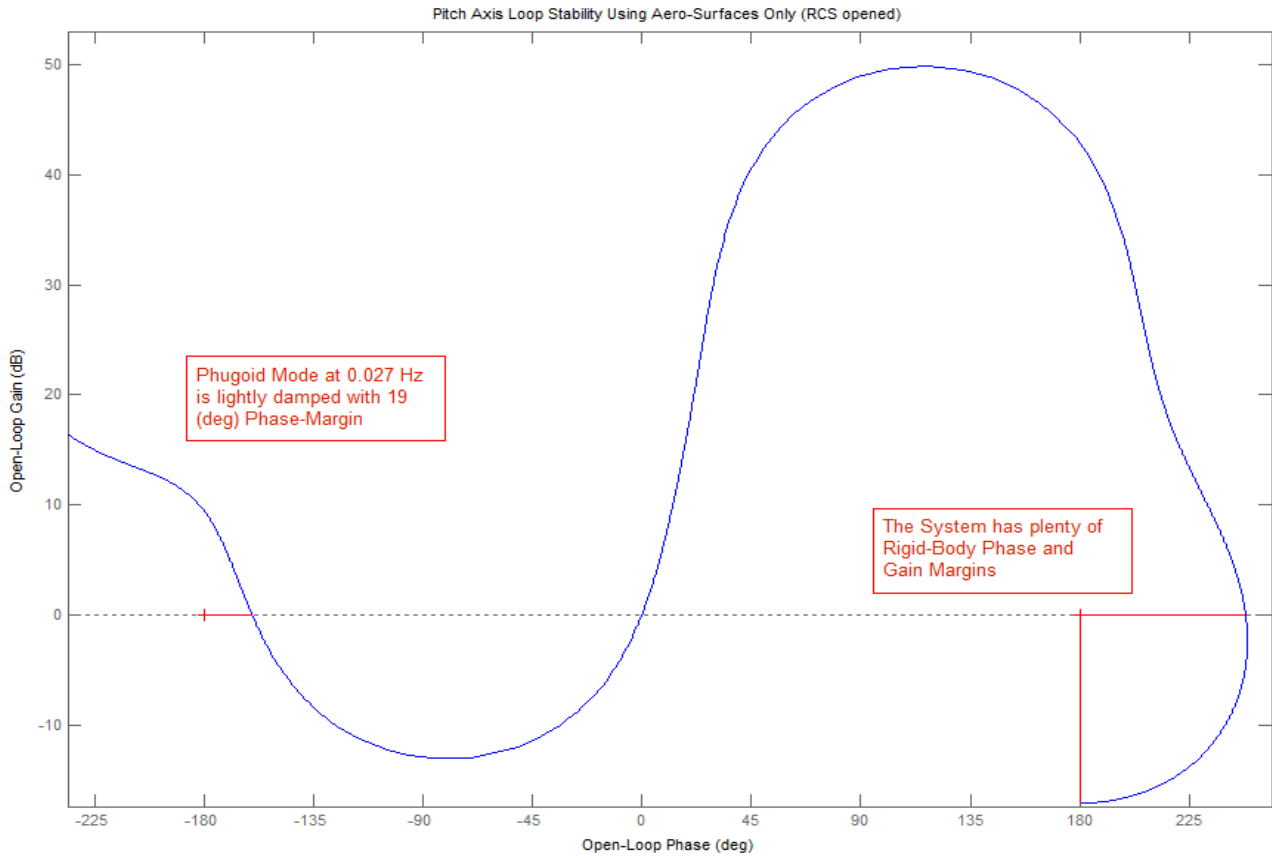
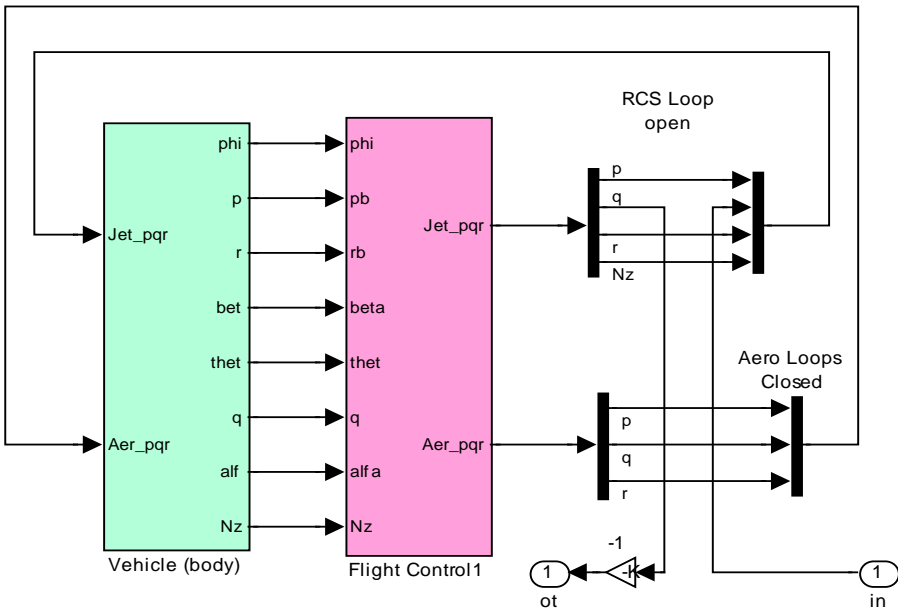


Figure (12) Nichols chart showing Pitch axis stability using the aero-surfaces only. The roll and yaw loops are closed. The RCS loops are opened. The rigid-body phase margin is 69 deg. The phase margin at the low frequency phugoid mode is 19 deg which implies what we already saw in the simulations, that the phugoid mode is lightly damped.



Pitch RCS Loop Stability Analysis

Figure (13) Linear Stability Analysis Model for the Pitch RCS loop with the Aero-Surfaces Closed

2.0 Flexible Vehicle Analysis

Our next objective is to introduce structural flexibility in the vehicle model. We will include 50 flexible modes and inertial coupling between surfaces and structure. Each mode is a structural resonance with a specific frequency that is excited differently from different excitation points (effector nodes) and also detected differently at different sensor points (sensor nodes). An assemblage of modes causes the structure to vibrate when it is excited either by forces, torques, or by the relative acceleration between hinged bodies. Aero-elasticity in the form of Generalized Aerodynamic Force Derivatives (GAFD) coefficients will also be included to couple aerodynamic forces with structural flexing. Inertial coupling coefficients will also be used to excite structural flexing due to surface slewing. We will also develop more advanced and complex simulation and analysis models including detailed actuator and sensor dynamics. The rigid-body control system gains developed in Section 1 will not be changed but flexibility filters will be included to attenuate some modal resonances that may induce unstable oscillations. The analysis will also include detailed modeling procedures, time-domain simulations, and frequency domain stability analysis.

2.1 Flexible Vehicle Model

The control system design and analysis thus far have been fairly straightforward but we have ignored a very important factor, structural flexibility, which usually tends to complicate stability and to decrease vehicle performance and control bandwidth. Structural flexibility on the Shuttle during reentry is excited mainly by the rotational accelerations of the aero-surfaces which create tail-wag-dog type of reaction forces and torques at the hinges. Variations in the angles of attack, sideslip, and in body rates they also cause aero-elastic coupling effects between aerodynamic forces and structure that further excite flexibility through the interaction with the control system and may cause flexure instabilities. Notice, that we are not addressing the flutter issue here because this is strictly an aero-structural problem and it does not involve the control system.

In this section we will describe how to generate a flexible vehicle system for stability analysis and simulation purposes. The input data file is: "*Shuttle_Entry_Flx.Inp*", and the flex analysis is performed in a separate folder "*C:\Flixan\ Examples\ Shuttle Hypersonic Re-Entry\Flex_Analysis*". The stability axes vehicle system with turn-coordination is not needed here because the basic control system was already designed in the previous section. The vehicle data in this file is almost identical to the rigid-body data-set. The modeling flags are set to "*Body Axes Output*" since we would like the output rates to be in the body axes. The "*No Turn Coordination*" flag is used, same as in the rigid-body simulation model. The GAFD flag is set to "*Include GAFD*" because we will include GAFD aero-elastic derivatives to couple aerodynamics with structure. In this configuration we will also turn-on the tail-wag-dog option in the control surfaces data. This flag is set to the right of: "*Number of control surfaces: 5*", by changing the "*No TWD*" flag to "*With TWD*". The tail-wag-dog dynamics generates reaction forces and torques due to surfaces slewing that excites both rigid and structure. This option creates additional inputs in the dynamic model, a total of five control surface accelerations is included in addition to the five surface deflections. Turning the TWD flag "on" it also creates five additional hinge moment outputs in the state-space model. The hinge moments represent the external loading at the surface hinge due to vehicle motion or aerodynamics. It does not include the actuator torque. These outputs are used as external loading torque inputs to the actuator models. They close mechanical load-torque feedback loops between the vehicle hinge moments outputs and the actuator external load inputs. They represent the actuator external loading generated due to aero-surface slewing and vehicle motion.

In the flex vehicle data-set we have also included some sensors, 3 gyros and 3 accelerometers. The 3 gyros are located in front of the vehicle CG and they are measuring roll, pitch, and yaw rates. The 3 accelerometers are in a different location, closer to the front of the vehicle measuring accelerations along the x, y, and z axes. Notice, that the accelerometers in the rigid body model were located at the vehicle CG. Notice, that when we do not specify an accelerometer in a rigid-body model the default acceleration output is three measurements at the CG, along: x, y, and z. Due to the offset the accelerometers in addition to translational accelerations, they also sense contributions caused by the vehicle rotational accelerations. The final item in the flex vehicle data-set that differs from the rigid body is the flex modes. The number of flex modes is defined near the bottom of the flex vehicle data-set and it is 50 modes, “*Number of Bending Modes: 50*”. The 50 modes are saved as a separate data-set in the input file. The input file may contain more than one set of modes for different applications. The title of the selected set of modes to be combined with the vehicle data is included at the bottom of the vehicle set, a line below the number of modes.

A selected set of modal data has already been created and it has been saved in the input data file “*Shuttle_Entry_Flx.Inp*” to be used in combination with the vehicle data for the preparation of the flex vehicle model. Its title is: “*Shuttle Early Hypersonic Atmospheric Re-Entry, First 50 Modes*” and it appears on the top of the modal data-set and is also included at the bottom of the vehicle data-set, as already described. It contains the mode shapes, slopes and frequencies of the 50 selected Nastran modes. The mode shapes and slopes in the selected set of modes correspond to important vehicle locations specified in the vehicle model, such as: aero-surface hinges, jet locations, gyros, and accelerometers. The reduced set of modes was extracted from a much bigger modal data set, from a separate file, that was generated by a finite elements program, such as Nastran. A mode-selection program was used in the process that is part of the Flixan package and selectable from the main menu. It compares the modal strengths and selects the strongest modes. In this case, however, we are not interested in the most dominant modes because we have already decided to use the first 50 flex modes. The units of the mode shapes and slopes are converted during the selection process to match the units of the vehicle data. The mode selection will be discussed in later sections, but first let’s talk about the data files needed for flexibility.

```

FLIGHT VEHICLE INPUT DATA .....
Space Shuttle Orbiter Flex Model during Early Re-Entry
! The following vehicle model is a Space Shuttle vehicle during the early phase of atmospheric
! re-entry where it is flying at a high angle of attack and it is using both RCS jets and
! control surfaces for attitude control. It uses an additional file (Shuttle_Orb.Gaf) which
! contains the GAFF and coupling coefficients in order to model the aeroelasticity effects.
!
Body Axes Output, Attitude=Euler Angles, Include GAFF, No Turn Coordination

Vehicle Mass (lb-sec^2/ft), Gravity Accelerat. (g) (ft/sec^2), Earth Radius (Re) (ft)      : 7460.4   32.17
Moments and products of Inertias Ixx, Iyy, Izz, Ixy, Ixz, Iyz, in (lb-sec^2-ft)         : 804000.0, 7325110.0,
CG location with respect to the Vehicle Reference Point, Xcg, Ycg, Zcg, in (feet)       : -82.85,   0.0,   2.7
Vehicle Mach Number, Velocity Vo (ft/sec), Dynamic Pressure (psf), Altitude (feet)     : 25.0   18640.0   4.0
Inertial Acceleration Vo_dot, Sensed Body Axes Accelerations Ax,Ay,Az (ft/sec^2)      : -7.39   -1.14   0.0000
Angles of Attack and Sideslip (deg), alpha, beta rates (deg/sec)                     : 40.0   0.0   -0.5
Vehicle Attitude Euler Angles, Phi_o,Thet_o,Psi_o (deg), Body Rates Po,Qo,Ro (deg/sec) : 0.0   39.15   0.0000
Wind Gust Vel wrt Vehi (Azim & Elev) angles (deg), or Force(lb), Torque(ft-lb), locat:xyz: Gust 45.0   90.0
Surface Reference Area (feet^2), Mean Aerodynamic Chord (ft), Wing Span in (feet)      : 2680.0   35.0,   79.0
Aero Moment Reference Center (Xmrc,Ymrc,Zmrc) Location in (ft), {Partial_rho/ Partial_H} : -81.36, 0.0, 2.97
Aero Force Coef/Deriv (1/deg), Along -X, {Cao,Ca_alf,PCa/PV,PCa/Ph,Ca_alfdot,Ca_g,Ca_bet}: 0.103, -0.007, -0.4e-6,
Aero Force Coeff/Derivat (1/deg), Along Y, {Cyo,Cy_bet,Cy_r,Cy_alf,Cy_p,Cy_betdot,Cy_V}: 0.0, -0.023, 0.39, 0.0,
Aero Force Coeff/Deriv (1/deg), Along Z, {Czo,Cz_alf,Cz_g,Cz_bet,PCz/Ph,Cz_alfdot,PCz/PV}: -2.6, -0.086, -1.7, 0.0,
Aero Moment Coeff/Deriv (1/deg), Pitch: {Cmo,Cm_alfa,Cm_alfdot,Cm_bet,Cm_g,PCm/PV,PCm/Ph}: 0.0012, -0.008, 0.0, 0.0,
Aero Moment Coeff/Derivat (1/deg), Yaw : {Cno, Cn_beta, Cn_betdot, Cn_p, Cn_r, Cn_alfa}: 0.0, -0.0011, 0.0,

Number of Control Surfaces, With or No TWD (Tail-Wags-Dog and Hinge Moment Dynamics) ?  : 5   With TWD

Control Surface No: 1                               Left Outbd Elevon
Trim Angle, Max/Min Deflection Angles from Trim, Hinge Line Angles: phi_h, lamda_h (deg): -5.0   30.0  -35.0  +2.5
Surface Mass, Inertia about Hinge, Moment Arm (Hinge to Surface CG), Surface Chord, Area : 55.0   227.4  1.8   6.322

```

```

Hinge Moment Derivatives (1/deg), { Chm_Alpha, Chm_Beta, Chm_Delta, Chm_Mach } : -0.0047 -0.00055 -0.0 0.0
Location of the Hinge Line Center with respect to Vehicle Reference (feet), {Xcs,Ycs,Zcs}: -118.6 -33.16 10.4
Forces (-x,y,z) due to Deflect. and Rates {Ca_del,Cy_del,Cz_del, Ca_deld,Cy_deld,Cz_deld}: 0.00022 -0.0018 -0.0062
Moments due to Deflections and Rates {Cl_del,Cm_del,Cn_del,Cl_deldot,Cm_deldot,Cn_deldot}: 0.0028 -0.0018 0.0006
Control Surface No: 2 Left Inbrd Elevon
Trim Angle, Max/Min Deflection Angles from Trim, Hinge Line Angles: phi_h, lamda_h (deg): -7.0 30.0 -35.0 +1.3
Surface Mass, Inertia about Hinge, Moment Arm (Hinge to Surface CG), Surface Chord, Area : 100.0 820.3 2.5 8.594
Hinge Moment Derivatives (1/deg), { Chm_Alpha, Chm_Beta, Chm_Delta, Chm_Mach } : -0.0047 -0.00055 -0.0097
Location of the Hinge Line Center with respect to Vehicle Reference (feet), {Xcs,Ycs,Zcs}: -118.6 -18.4 11.1
Forces (-x,y,z) due to Deflect. and Rates {Ca_del,Cy_del,Cz_del, Ca_deld,Cy_deld,Cz_deld}: 0.00025 -0.0009 -0.008
Moments due to Deflections and Rates {Cl_del,Cm_del,Cn_del,Cl_deldot,Cm_deldot,Cn_deldot}: 0.0006 -0.0032 0.0001
Control Surface No: 3 Right Inbd Elevon
Trim Angle, Max/Min Deflection Angles from Trim, Hinge Line Angles: phi_h, lamda_h (deg): -7.0 30.0 -35.0 -1.3
Surface Mass, Inertia about Hinge, Moment Arm (Hinge to Surface CG), Surface Chord, Area : 100.0 785.0 2.5 8.594
Hinge Moment Derivatives (1/deg), { Chm_Alpha, Chm_Beta, Chm_Delta, Chm_Mach } : -0.0047 -0.00055 -0.0097
Location of the Hinge Line Center with respect to Vehicle Reference (feet), {Xcs,Ycs,Zcs}: -118.6 18.4 11.1
Forces (-x,y,z) due to Deflect. and Rates {Ca_del,Cy_del,Cz_del, Ca_deld,Cy_deld,Cz_deld}: 0.00025 0.0009 -0.008 0.0
Moments due to Deflections and Rates {Cl_del,Cm_del,Cn_del,Cl_deldot,Cm_deldot,Cn_deldot}: -0.0006 -0.0032 -0.0001
Control Surface No: 4 Right Outbd Elevon
Trim Angle, Max/Min Deflection Angles from Trim, Hinge Line Angles: phi_h, lamda_h (deg): -5.0 30.000 -35.0 -2.5
Surface Mass, Inertia about Hinge, Moment Arm (Hinge to Surface CG), Surface Chord, Area : 55.0 227.4 1.8 6.322
Hinge Moment Derivatives (1/deg), { Chm_Alpha, Chm_Beta, Chm_Delta, Chm_Mach } : -0.0047 0.00055 -0.0097
Location of the Hinge Line Center with respect to Vehicle Reference (feet), {Xcs,Ycs,Zcs}: -118.6 33.16 10.4
Forces (-x,y,z) due to Deflect. and Rates {Ca_del,Cy_del,Cz_del, Ca_deld,Cy_deld,Cz_deld}: 0.00022 0.0018 -0.0062
Moments due to Deflections and Rates {Cl_del,Cm_del,Cn_del,Cl_deldot,Cm_deldot,Cn_deldot}: -0.0028 -0.0018 -0.0006

Number of Thruster Engines, Include or Not the Tail-Wags-Dog and Load-Torque Dynamics ? : 11

RCS Jet No: 1 Back, Left, Up, +Z (three 800 lb jets) : BLU Jet Throttling Node 16
Engine Nominal Thrust, and Maximum Thrust in (lb) (for throttling) : 0.0 2400.0
Mounting Angles wrt Vehicle (Dyn,Dzn), Maximum Deflections from Mount (Dymax,Dzmax) (deg): -88.5 39.3 0.0 0.0
Eng Mass (slug), Inertia about Gimbal (lb-sec^2-ft), Moment Arm, engine CG to gimbal (ft): 1.0 1.0 1.0
Thruster location with respect to the Vehicle Reference Axes, Xgimb, Ygimb, Zgimb, (ft): -128.1, -11.5, -5.8
RCS Jet No: 2 Back, Right, Up, +Z (three 800 lb jets) : BRU Jet Throttling Node 11
Engine Nominal Thrust, and Maximum Thrust in (lb) (for throttling) : 0.0 2400.0
Mounting Angles wrt Vehicle (Dyn,Dzn), Maximum Deflections from Mount (Dymax,Dzmax) (deg): -88.5 -131.3 0.0 0.0
Eng Mass (slug), Inertia about Gimbal (lb-sec^2-ft), Moment Arm, engine CG to gimbal (ft): 1.0 1.0 1.0
Thruster location with respect to the Vehicle Reference Axes, Xgimb, Ygimb, Zgimb, (ft): -128.1, 11.5, -5.8
RCS Jet No: 3 Back, Left, Down, -Z (three 800 lb jets) : BLD Jet Throttling Node 17
Engine Nominal Thrust, and Maximum Thrust in (lb) (for throttling) : 0.0 2400.0
Mounting Angles wrt Vehicle (Dyn,Dzn), Maximum Deflections from Mount (Dymax,Dzmax) (deg): +82.5 89.3 0.0 0.0
Eng Mass (slug), Inertia about Gimbal (lb-sec^2-ft), Moment Arm, engine CG to gimbal (ft): 1.0 1.0 1.0
Thruster location with respect to the Vehicle Reference Axes, Xgimb, Ygimb, Zgimb, (ft): -128.7, -10.2, -2.23
RCS Jet No: 4 Back, Right, Down, -Z (three 800 lb jets) : BRD Jet Throttling Node 12
Engine Nominal Thrust, and Maximum Thrust in (lb) (for throttling) : 0.0 2400.0
Mounting Angles wrt Vehicle (Dyn,Dzn), Maximum Deflections from Mount (Dymax,Dzmax) (deg): +82.4 -89.2 0.0 0.0
Eng Mass (slug), Inertia about Gimbal (lb-sec^2-ft), Moment Arm, engine CG to gimbal (ft): 1.0 1.0 1.0
Thruster location with respect to the Vehicle Reference Axes, Xgimb, Ygimb, Zgimb, (ft): -128.7, 10.2, -2.23
RCS Jet No: 5 Back, Left, +Y (three 800 lb jets) : BL+Y Jet Throttling Node 18
Engine Nominal Thrust, and Maximum Thrust in (lb) (for throttling) : 0.0 2400.0
Mounting Angles wrt Vehicle (Dyn,Dzn), Maximum Deflections from Mount (Dymax,Dzmax) (deg): 0.5 +88.5 0.0 0.0
Eng Mass (slug), Inertia about Gimbal (lb-sec^2-ft), Moment Arm, engine CG to gimbal (ft): 1.0 1.0 1.0
Thruster location with respect to the Vehicle Reference Axes, Xgimb, Ygimb, Zgimb, (ft): -131.2, -12.2, -3.5
RCS Jet No: 6 Back, Right, -Y (three 800 lb jets) : BR-Y Jet Throttling Node 13
Engine Nominal Thrust, and Maximum Thrust in (lb) (for throttling) : 0.0 2400.0
Mounting Angles wrt Vehicle (Dyn,Dzn), Maximum Deflections from Mount (Dymax,Dzmax) (deg): 0.5 -88.5 0.0 0.0
Eng Mass (slug), Inertia about Gimbal (lb-sec^2-ft), Moment Arm, engine CG to gimbal (ft): 1.0 1.0 1.0
Thruster location with respect to the Vehicle Reference Axes, Xgimb, Ygimb, Zgimb, (ft): -131.2, 12.2, -3.5

Number of Gyros, (Attitude and Rate), Node 38 : 3
Gyro No 1 Axis:(Pitch,Yaw,Roll), (Attitude or Rate), Location in Vehicle Axes (feet) : Roll Rate -48.4, 0.0,
Gyro No 2 Axis:(Pitch,Yaw,Roll), (Attitude or Rate), Location in Vehicle Axes (feet) : Pitch Rate -48.4, 0.0,
Gyro No 3 Axis:(Pitch,Yaw,Roll), (Attitude or Rate), Location in Vehicle Axes (feet) : Yaw Rate -48.4, 0.0,
Number of Accelerometers, (x,y,z) : 3
Acceleromet No 1 Axis:(X,Y,Z), (Acceleration, Flex_Posit, Flex_Veloc, Flex_Accel), Locat(ft): X-axis Acceler -32.2, 0.0,
Acceleromet No 2 Axis:(X,Y,Z), (Acceleration, Flex_Posit, Flex_Veloc, Flex_Accel), Locat(ft): Y-axis Acceler -32.2, 0.0,
Acceleromet No 3 Axis:(X,Y,Z), (Acceleration, Flex_Posit, Flex_Veloc, Flex_Accel), Locat(ft): Z-axis Acceler -32.2, 0.0,
Number of Vane Sensors, (Alpha or Beta) : 0

Number of Slosh Modes : 0

Number of Bending Modes : 50
Shuttle Early Hypersonic Atmospheric Re-Entry, First 50 Modes
Selected GAFD Mode Numbers from GAFD File : 1 2 3 4 5 6 7 8 9 ... 50
Selected GAFD Surface Numbers from GAFD File : 1 2 3 4 5
-----

```

SELECTED MODAL DATA AND LOCATIONS FOR ALL AXES

Shuttle Early Hypersonic Atmospheric Re-Entry, First 50 Modes

! The first 50 flex modes were selected that correspond to the GAFD frequencies

MODE #	1/	Frequency (rad/sec)	Damping (zeta)	Generalized Mass=	9.1779	0.50000E-02	7714.4		
DEFINITION OF LOCATIONS (NODES)				phi along X	phi along Y	phi along Z	sigm about X	sigm about Y	sigm
Modal Data at the 5 Control Surfaces (Hinges)									
Left Outboard Elevon Hinge Li	1726	-0.38329D-01	0.32463D-02	0.45568D-01	-0.59548D-04	-0.89157D-03			
Left Inboard Elevon Hinge Lin	1721	-0.39217D-01	0.32014D-02	0.44843D-01	0.00000D+00	0.00000D+00			
Right Inboard Elevon Hinge Li	1571	-0.40218D-01	-0.55768D-02	0.45595D-01	0.00000D+00	0.00000D+00			
Right Outboard Elevon Hinge L	1576	-0.40174D-01	-0.56246D-02	0.47212D-01	0.12074D-03	-0.90312D-03			
RUDDER NO.1 HINGE TAIL	2376	-0.51453D-02	-0.68149D-03	0.32814D-01	0.00000D+00	0.00000D+00			
Modal Data at the 11 Engines, (x,y,z)...									
RCS THRUST POINT (BLU)	1963	-0.18018D-01	-0.10362D-02	0.30835D-01	0.00000D+00	0.00000D+00			
RCS THRUST POINT (BRU)	1893	-0.18538D-01	-0.81625D-03	0.31420D-01	0.00000D+00	0.00000D+00			
RCS THRUST POINT (BLD)	1967	-0.21845D-01	-0.12074D-02	0.29622D-01	0.00000D+00	0.00000D+00			
RCS THRUST POINT (BRD)	1897	-0.22273D-01	-0.86932D-03	0.30108D-01	0.00000D+00	0.00000D+00			
RCS THRUST POINT (BL+Y)	1969	-0.20146D-01	-0.11740D-02	0.27158D-01	0.00000D+00	0.00000D+00			
RCS THRUST POINT (BR-Y)	1899	-0.20741D-01	-0.92556D-03	0.27822D-01	0.00000D+00	0.00000D+00			
RCS THRUSTER (FU)	2988	-0.17500D-02	0.18328D-02	0.30856D+00	0.00000D+00	0.00000D+00			
RCS THRUSTER (FLD & FRD)	2945	-0.18498D-02	0.18263D-02	0.30874D+00	0.00000D+00	0.00000D+00			
RCS THRUSTER (FLD & FRD)	2945	-0.18498D-02	0.18263D-02	0.30874D+00	0.00000D+00	0.00000D+00			
RCS THRUSTER (FL-Y)	2987	-0.21360D-01	0.14524D-02	0.30226D+00	0.00000D+00	0.00000D+00			
RCS THRUSTER (FR+Y)	2944	-0.21701D-01	0.18937D-02	0.30271D+00	0.00000D+00	0.00000D+00			
Modal Data at the 3 Gyros ...									
RATE GYRO (for control)	1490	-0.44093D-01	0.12177D-02	0.20418D+00	0.35437D-03	-0.38225D-02			
RATE GYRO (for control)	1490	-0.44093D-01	0.12177D-02	0.20418D+00	0.35437D-03	-0.38225D-02			
RATE GYRO (for control)	1490	-0.44093D-01	0.12177D-02	0.20418D+00	0.35437D-03	-0.38225D-02			
Modal Data at the 3 Accelerometers, along (x,y,z)...									
CABIN ACCEL FWD BKHD (for con	307	0.00000D+00	0.17707D-02	0.30067D+00					
CABIN ACCEL FWD BKHD (for con	307	0.00000D+00	0.17707D-02	0.30067D+00					
CABIN ACCEL FWD BKHD (for con	307	0.00000D+00	0.17707D-02	0.30067D+00					
Modal Data at the Disturbance Point									
ENG.1 GIMBAL	2077	-0.21664D-01	-0.82916D-03	0.40440D-01	0.68930D-05	-0.11568D-02			

2.2 Flex Data Files

Three types of data files are required for the implementation of structural flexibility, including aero-elasticity in Flixan: a modal data file, aero-elasticity data, and a nodes map.

Modal Data: The modal data file “*Shuttle_Orb.Mod*” is a big file that contains in general all the flex modes created by the Nastran program. In this case, however, it is not very big and it contains mode shapes and frequencies for the first 80 modes. The first two lines are titles. The next line includes the number of modes and vehicle locations, 80 modes and 40 nodes. This file includes 80 frames of data, a frame for each mode. All 80 frames have the same structure. The first line in each frame includes the modal frequency in (rad/sec), the damping coefficient (ζ), and the modal mass in (lb-sec²/inch). The following lines in each frame consist of 7 columns. Each line corresponds to a node. The first column identifies the locations (nodes), the next 3 columns are the generalized modal displacements which are three translations along x, y, z, and the next 3 columns are the modal slopes, three rotations about x, y, z. They are calculated at 40 vehicle locations (nodes) which are probably a lot more than the locations needed for modeling defined in the vehicle data. It is a good practice when you request modal data from structures people to ask for more nodes than you think you will need, in case you will may need them at a later time because of an unexpected modification in the design. It is easier for a structures person to add a few more points up front than to go back and modify the finite elements model.

Vehicle structure locations are associated with a node id number that is created by the FEM program. In this case there are 40 node ids included in the first column. The node ids are defined in the nodes map file. The damping coefficients and the modal masses are the same in this case for all modes and they are set to: $\zeta=0.005$, and $m_g=642.87$ (lb-sec²/inch). The mode shapes are normalized by a constant

modal mass which is almost equal to the vehicle mass. This modal data file is used as input to the mode-selection program which selects a smaller set of modes, as we already discussed, with fewer nodes at locations that correspond to the vehicle data. The reduced set of modes is also scaled by the mode-selection program to be compatible with the units and directions defined in the vehicle data. The selected and scaled set of modes are saved in file “*Shuttle_Entry_Flx.Inp*” to be processed by the flex vehicle modeling program.

Modal Data File "Shuttle_Orb.Mod"

Structural Modal Data for ... (units are in pounds and inches)

Space Shuttle Orbiter Vehicle During Entry

NUMBER OF MODES, NUMBER OF NODES : 80, 40

Mode Number,	Frequency (rad/sec),	Damping (zeta),	Generalized Mass (slug):	1	9.1779	0.005	642.87
Node ID:	Along X	Along Y	Along Z	About X	About Y	About Z	
294	0.000000D+00	0.468367D-02	-0.795743D+00	0.000000D+00	0.000000D+00	0.000000D+00	
3504	0.000000D+00	0.333529D-03	-0.793648D+00	0.000000D+00	0.000000D+00	0.000000D+00	
352	0.265984D-01	0.100059D+00	0.384304D+00	0.000000D+00	0.000000D+00	0.000000D+00	
369	0.262976D-01	-0.998114D-01	0.385536D+00	0.000000D+00	0.000000D+00	0.000000D+00	
411	0.237531D-01	0.165316D+00	-0.282369D-01	0.000000D+00	0.000000D+00	0.000000D+00	
418	0.234281D-01	-0.164964D+00	-0.277417D-01	0.000000D+00	0.000000D+00	0.000000D+00	
2169	0.386642D-01	0.000000D+00	0.000000D+00	0.336726D-05	-0.651870D-04	-0.152503D-04	
2173	0.387766D-01	0.000000D+00	0.000000D+00	-0.748488D-05	-0.663426D-04	0.997418D-05	
1886	0.192967D-01	-0.892515D-03	-0.287889D-01	0.000000D+00	0.000000D+00	0.000000D+00	
1890	0.207408D-01	-0.861926D-03	-0.301258D-01	0.000000D+00	0.000000D+00	0.000000D+00	
1893	0.185376D-01	-0.816255D-03	-0.314201D-01	0.000000D+00	0.000000D+00	0.000000D+00	
1897	0.222735D-01	-0.869319D-03	-0.301079D-01	0.000000D+00	0.000000D+00	0.000000D+00	
1899	0.207408D-01	-0.925557D-03	-0.278218D-01	0.000000D+00	0.000000D+00	0.000000D+00	
1956	0.187557D-01	-0.110340D-02	-0.281826D-01	0.000000D+00	0.000000D+00	0.000000D+00	
1959	0.201455D-01	-0.112284D-02	-0.307635D-01	0.000000D+00	0.000000D+00	0.000000D+00	
1963	0.180177D-01	-0.103621D-02	-0.308355D-01	0.000000D+00	0.000000D+00	0.000000D+00	
1967	0.218445D-01	-0.120740D-02	-0.296220D-01	0.000000D+00	0.000000D+00	0.000000D+00	
1969	0.201455D-01	-0.117401D-02	-0.271582D-01	0.000000D+00	0.000000D+00	0.000000D+00	
2420	0.381235D-01	-0.158861D-02	-0.248556D-01	0.000000D+00	0.000000D+00	0.000000D+00	
2077	0.216639D-01	-0.829165D-03	-0.404404D-01	-0.574416D-06	-0.964041D-04	-0.818756D-06	
2080	0.333059D-01	-0.122723D-02	-0.379932D-01	-0.453544D-05	-0.787697D-04	-0.354365D-05	
2243	0.329084D-01	-0.119877D-02	-0.374159D-01	-0.237023D-05	-0.973202D-04	-0.371943D-05	
1571	0.402185D-01	-0.557683D-02	-0.455948D-01	0.000000D+00	0.000000D+00	0.000000D+00	
1806	0.395075D-01	-0.172486D-02	-0.428881D-01	0.000000D+00	0.000000D+00	0.000000D+00	
1576	0.401741D-01	-0.562461D-02	-0.472122D-01	-0.100620D-04	-0.752599D-04	0.616989D-06	
1818	0.399342D-01	-0.134595D-02	-0.464264D-01	0.000000D+00	0.000000D+00	0.000000D+00	
1721	0.392166D-01	0.320142D-02	-0.448427D-01	0.000000D+00	0.000000D+00	0.000000D+00	
1826	0.385146D-01	-0.737673D-03	-0.419497D-01	0.000000D+00	0.000000D+00	0.000000D+00	
1726	0.383289D-01	0.324626D-02	-0.455683D-01	0.496230D-05	-0.742973D-04	-0.543323D-05	
1839	0.378889D-01	-0.943030D-03	-0.425513D-01	0.000000D+00	0.000000D+00	0.000000D+00	
2944	0.217011D-01	0.189369D-02	-0.302712D+00	0.000000D+00	0.000000D+00	0.000000D+00	
2945	0.184976D-02	0.182632D-02	-0.308738D+00	0.000000D+00	0.000000D+00	0.000000D+00	

Nodes Map:

The nodes map file is a look-up table that helps the analyst identify the vehicle locations in the modal data file. The nodes file in this example is “*Shuttle_Orb.Nod*”. This table begins with a title on the top followed by a list of nodes in columns. The left column includes a short description of each node in the sequence that they appear in the modal data file (.Mod). The second column is the node number (1 to 40) in ascending sequence (not the node id). The third column is the node id which is a large number (typically 4-5 digits long) for node identification created from the finite elements program. The next 3 columns represent the x, y, z location in vehicle coordinates for each node. The map file is used as a look-up table by the mode selection program. The list of nodes pops-up in window menus when running the program interactively. The analyst uses those menus to select vehicle locations which are associated with structural nodes, shapes and slopes in the modal data file and used to perform mode strength comparison between structural points and in selecting flex modes.

Nodes Map File "Shuttle_Orb.Nod"

Shuttle Orbiter Nodes List

Node Description	Node No	Nastran ID	Node Location X,Y,Z (feet)		
COULOMB DMP.PT.ON PYLD	1	294	-103.8	6.989	-34.50
COULOMB DMP.PT.ON PYLD	2	3504	-103.8	-6.989	-34.50
V-Square DAMPER Point	3	352	-93.02	6.710	-32.18
V-Square DAMPER Point	4	369	-93.02	-6.710	-32.18
V-Square DAMPER Point	5	411	-93.02	7.292	-33.34
V-Square DAMPER Point	6	418	-93.02	-7.292	-33.34
RATE GYRO 1	7	2169	-108.6	-1.750	-24.60
RATE GYRO 4	8	2173	-108.6	1.750	-24.60
RCS THRUST POINT	9	1886	-129.6	11.42	-39.42
RCS THRUST POINT	10	1890	-128.5	12.49	-38.25
RCS THRUST POINT (BRU)	11	1893	-127.4	11.00	-40.04
RCS THRUST POINT (BRD)	12	1897	-128.5	9.172	-36.88
RCS THRUST POINT (BR-Y)	13	1899	-130.4	12.49	-38.25
RCS THRUST POINT	14	1956	-129.6	-11.42	-39.42
RCS THRUST POINT	15	1959	-127.4	-12.49	-38.25
RCS THRUST POINT (BLU)	16	1963	-127.4	-11.00	-40.04
RCS THRUST POINT (BLD)	17	1967	-128.5	-9.172	-36.88
RCS THRUST POINT (BL+Y)	18	1969	-130.4	-12.49	-38.25
BODY FLAP	19	2420	-132.1	-0.8333	-24.12
ENG.1 GIMBAL	20	2077	-120.4	0.000	-36.92
ENG.3 GIMBAL	21	2080	-122.3	4.417	-28.55
ENG.2 GIMBAL	22	2243	-122.3	-4.417	-28.55
Right Inboard Elevon Hinge Line	23	1571	-115.6	17.59	-23.38
INBOARD ELEVON R	24	1806	-118.5	17.53	-24.05
Right Outboard Elevon Hinge Line	25	1576	-115.6	32.16	-24.72
OTBOARD ELEVON R	26	1818	-117.4	36.08	-25.30
Left Inboard Elevon Hinge Line	27	1721	-115.6	-17.59	-23.38
INBOARD ELEVON L	28	1826	-118.5	-17.53	-24.05
Left Outboard Elevon Hinge Line	29	1726	-115.6	-32.16	-24.72
OTBOARD ELEVON L	30	1839	-119.7	-36.08	-25.27
RCS THRUSTER (FR+Y)	31	2944	-30.39	5.971	-29.93
RCS THRUSTER (FLD & FRD)	32	2945	-29.24	1.199	-34.45

Generalized Aero Force Derivative (GAFD) Coefficients:

As we mentioned earlier the excitation of the structural equations in Flixan can be implemented either (a) with external forces and torques at the hinges using modal shapes and slopes or (b) by means of inertial coupling coefficients which couple the surface rotational acceleration with the bending modes and including GAFD, aero-elastic coefficients that couple the aerodynamic forces generated by the vehicle motion to the structure. The first method uses modal shapes and slopes at the hinges. It assumes that flexibility is excited by rigid surface rotations and that the aero forces at the hinges are generated by flat panel rotations from their nominal positions. In this example we will use the second method which is more complex to implement because it requires additional data to be generated but a lot more accurate dynamically.

The GAFD coefficients are obtained from the structures group where they combine the finite element models with aerodynamics and they examine for possible flutter issues. The GAFD data and the inertial coupling coefficients have been calculated for the first 50 modes and are included in file "Shuttle_Orb.Gaf". GAFD filenames have an extension (.Gaf) to be recognized by the Flixan program. The data was post-processed and reformatted from an original structures file in the form shown in file "Shuttle_Orb.Gaf". The flight vehicle modeling program recognizes the GAFD option when the "Include GAFD" flag is set in the flags line which is on the top of the vehicle data-set below the title. Otherwise, the default "Without GAFD" option will be implemented using modal data at the aero-surface hinges. However, we still need the modal data set for the sensor nodes.

The GAFD file includes aero-elasticity derivatives at frequencies that correspond to the first 50 flexible modes. For this reason in this example we will include the first 50 flexible modes. The GAFD file in addition to aero-elasticity derivatives it also contains the Inertial Coupling Coefficients. They are the off-diagonal blocks in the Nastran mass matrix that couple the aero-surface accelerations with flexibility. They are described by the hinge moment equations in the flex equations document and they are also called “*H-Parameters*”. The coupling occurs in both directions, surface accelerations exciting flexibility and flexibility creating torques at the hinges, due to the reaction forces alone, not the aerodynamics.

Now let us take a look inside file “*Shuttle_Orb.Gaf*”. The second line (below the title) indicates that there are five rigid body directions (alpha, beta, p, q, and r). These are the rigid vehicle variables that will induce aero-forces that will in turn excite flexibility. There are also 50 frequencies that correspond to the 50 flex modes, and there are five control surfaces that will also excite flex. In the next line we must define four parameters that are used in the normalization of the GAFD data, the Mach number, the vehicle velocity, the vehicle reference area, and the reference length. In the next few lines we include parameters related with the control surfaces, the reference areas in (ft²), their reference lengths in (ft), and their moments of inertia about the hinge in (slug-ft²). The aero-surfaces must be defined in the same order as in the vehicle data. In the next line we include the 50 GAFD frequencies that should correspond to the first 50 flex mode frequencies. The next group of data is a (5x50) matrix which is the inertial coupling coefficients that couple the 5 control surfaces with the 50 flex modes. They should be in the same order as in the vehicle data. The aero-elastic data have been extracted from the double lattice matrices. They are divided into two main categories: displacements and rates matrices.

From the displacements lattice matrix we have extracted a group of aero-elastic derivatives that define how the aerodynamic forces and moments vary as a function of generalized modal deflections ($\eta_{(j)}$, $j=1:50$). They define how the aero forces and moments vary with flex displacements. The next group of data describes the opposite. It defines how each mode gets excited by a variation in alpha, beta, p, q, or r. The next group of data is a (50x50) matrix that defines coupling between modes due to modal displacements. Then we have data that define modal excitations due to deflections of the five surfaces and the aero forces. The next group of data are hinge moment coefficients due to vehicle displacements from nominal (alpha, beta, p, q, r). We also have hinge moment coefficients due modal displacements, and hinge moment coefficients due to surface deflections.

From the rates lattice matrix we have extracted a group of aero-elastic derivatives that define how the aerodynamic forces and moments vary as a function of generalized modal rates ($\eta_{\text{-dot}(j)}$, $j=1:50$), in other words, how the aero forces and moments vary with flexure rates. The next group of data describes the opposite, which is how each mode gets excited by the derivatives of: alpha, beta, p, q, or r. The next group of data is a (50x50) matrix that defines coupling between modes caused by modal rates. Then we have data that define modal excitations due to angular rates of the five surfaces. The next group of data defines hinge moment coefficients due to vehicle rates: (alpha-dot, beta-dot, p-dot, q-dot, r-dot). We also have hinge moment coefficients due modal rates, and hinge moment coefficients due to surface angular rates.

The following equation describes how the flex modes are excited by aero-surface accelerations via the inertial coupling coefficients. They are also excited by (α , β , body rates, and surface deflections), and their rates, via the aero-elastic coefficients. The second equation describes how the aero-surface hinge

moments are created by (α , β , body rates, surface deflections), and their rates, via the hinge moment coefficients, and also due to flexibility via the inertial coupling coefficients $h_s(k,j)$.

$$m_g(j) \left(s^2 + 2\zeta_j \omega_j s + \omega_j^2 \right) \eta_j(s) = - \sum_{l=1}^{N_{surf}} h_s(l, j) \ddot{\delta}_s(l) \\ + \bar{Q} S_{ref}^* \left[\begin{aligned} &+ C_{\eta_j \alpha} \alpha_w + C_{\eta_j \beta} \beta_w + \left(\frac{l_{ch}^*}{2V_0} \right) (C_{\eta_j \dot{\alpha}} \dot{\alpha}_w + C_{\eta_j q} q) + \left(\frac{l_{ch}^*}{2V_0} \right)^2 C_{\eta_j \dot{q}} \dot{q} \\ &+ \left(\frac{l_{sp}^*}{2V_0} \right) (C_{\eta_j \dot{\beta}} \dot{\beta}_w + C_{\eta_j p} p + C_{\eta_j r} r) + \left(\frac{l_{sp}^*}{2V_0} \right)^2 (C_{\eta_j \dot{p}} \dot{p} + C_{\eta_j \dot{r}} \dot{r}) \\ &+ \sum_{k=1}^{N_{surf}} \left[C_{\eta_j \delta_s} \delta_s(k) + C_{\eta_j \dot{\delta}_s} \left(\frac{\bar{c}_{sk}}{2V_0} \right) \dot{\delta}_s(k) \right] + \sum_{i=1}^{N_{mode}} \left[C_{\eta_j \eta_i} \eta_i + \left(\frac{C_{\eta_j \dot{\eta}_i}}{V_0} \right) \dot{\eta}_i \right] \end{aligned} \right]$$

Equation showing how modal displacements for a mode (j) are excited by aero-surfaces and the vehicle motion

$$M_{hs}(k) = \text{Terms due to rigid vehicle motion} - \sum_{j=1}^{N_{mod}} [h_s(k, j) \ddot{\eta}(j)] \\ + \bar{Q} S_{sk} \bar{c}_{sk} \left[C_{h\alpha k} \alpha_w + C_{h\beta k} \beta_w + \left(\frac{l_{ch}^*}{2V_0} C_{h\dot{\alpha} k} \dot{\alpha}_w + \frac{l_{sp}^*}{2V_0} C_{h\dot{\beta} k} \dot{\beta}_w \right) \right] \\ + \bar{Q} S_{sk} \bar{c}_{sk} \left[\left(\frac{l_{ch}^*}{2V_0} C_{hkq} q + \frac{l_{sp}^*}{2V_0} (C_{hkp} p + C_{hkr} r) \right) + \left(\left(\frac{l_{ch}^*}{2V_0} \right)^2 C_{hk\dot{q}} \dot{q} + \left(\frac{l_{sp}^*}{2V_0} \right)^2 (C_{hk\dot{p}} \dot{p} + C_{hk\dot{r}} \dot{r}) \right) \right] \\ + \bar{Q} S_{sk} \bar{c}_{sk} \sum_{l=1}^{N_{Surf}} \left[C_{h\delta(k,l)} \delta_s(l) + \left(\frac{\bar{c}_{s(l)}}{2V_0} \right) C_{h\dot{\delta}(k,l)} \dot{\delta}_s(l) \right] \\ + \bar{Q} S_{sk} \bar{c}_{sk} \sum_{j=1}^{N_{Mode}} \left[C_{h\eta(k,j)} \eta(j) + \left(\frac{C_{h\dot{\eta}(k,j)}}{V_0} \right) \dot{\eta}(j) \right]$$

Equation describing how the Aero-Surface Hinge Moments are created by (α , β , body rates, surface deflections and rates) via the hinge moment coefficients and also due to flexibility via the inertial coupling coefficients.

Where:

S_{ref}^* is the aerodynamic surface area in (ft²) used to scale the GAFD data. It may not be the same as the vehicle surface reference area S_{ref} .

l_{ch}^*, l_{sp}^* are the reference chord and span in (ft) used to normalize the GAFD data. It may not be the same as the chord or span (l_{ch}, l_{sp}) used in the rigid body equations.

c_{sk} is the control surface (k) reference length in (feet) to normalize the GAFD data.

$\delta_{s(k)}$ is the clockwise rotation in (radians) of a control surface (k) about its hinge vector. The rotation is only due to actuator displacement and it does not include structural flexibility.

$h_s(k,j)$ are the inertial coupling coefficients (h-parameters) in (lb-sec²) that couple mode (j) excitation to surface (k) acceleration.

η_i is the generalized modal displacement in (feet) of a flex mode (j).

The following define the aero-elastic and hinge-moment coefficients:

$Cm\eta_j$	pitching moment increment due to mode (j) generalized displacement
$Cy\eta_j$	side-force increment due to mode (j) generalized displacement
$C\eta_j\alpha$	mode (j) excitation due an increment in the angle of attack
$C\eta_j p$	mode (j) excitation due an increment in roll rate
$C\eta_j\eta_k$	mode (j) excitation due to an increment of a mode (k) displacement
$C\eta_j\delta_k$	mode (j) excitation due to aero-surface (k) deflection
$Cm\dot{\eta}_j$	pitching moment increment due to mode (j) displacement rate
$Cy\dot{\eta}_j$	side-force increment due to mode (j) displacement rate
$C\eta_j\dot{\alpha}$	mode (j) excitation due an increment in the rate of angle of attack
$C\eta_j\dot{p}$	mode (j) excitation due an increment in roll acceleration
$C\eta_j\dot{\eta}_k$	mode (j) excitation due to an increment of a mode (k) displacement rate
$C\eta_j\dot{\delta}_k$	mode (j) excitation due to aero-surface (k) deflection rate
$Ch_k\alpha$	hinge moment at surface (k) due an increment in the angle of attack
$Ch_k r$	hinge moment at surface (k) due an increment in the yaw rate
$Ch_k\eta_j$	hinge moment at surface (k) due an increment of a mode (j) displacement
$Ch_k\delta_l$	hinge moment at surface (k) due a surface (l) deflection increment
$Ch_k\dot{\alpha}$	hinge moment at surface (k) due an increment in the rate of angle of attack
$Ch_k\dot{r}$	hinge moment at surface (k) due an increment in the yaw acceleration
$Ch_k\dot{\eta}_j$	hinge moment at surface (k) due an increment of a mode (j) displacement rate
$Ch_k\dot{\delta}_l$	hinge moment at surface (k) due a surface (l) deflection rate

The following GAFD file below includes the inertial coupling coefficients, the aero-elastic coefficients, and the hinge-moment coefficients for the 5 surfaces and the first 50 flex modes.

H-Parameters and GAFD File "Shuttle_Orb.Nod"

GENERALIZED AERO FORCE DERIVATIVES (GAFD) and INERTIAL COUPLING PARAMETERS (H-param) Data for the Shuttle Entry

Number of: Rigid Body Vehicle Degrees of Freedom, Flexible Modes, Control Surfaces= 5 50 5
Mach No, Velocity (ft/sec), Vehicle Reference Area (ft²), Aerodynamic Chord (ft) = 25.0 18000.0 26900.0 39.56
Control Surface Reference Areas in (ft²) {2 Outboard/Inboard Elevons, Rudder} = 75.82 134.96 134.96 75.82
Control Surface Reference Chords in (feet) {2 Outboard/Inboard Elevons, Rudder} = 6.322 8.59 8.594 6.322 6.1
Moments of Inertia of the Control Surfaces about the Hinge, (ft-lb-sec²) = 227.4 820.3 785.0 227.4 254.38
Modal Frequencies in (radian/sec) = 0.91779E+01 0.94122E+01

INERTIAL COUPLING PARAMETERS in (lb-sec²-ft)

Inertial Coupling (H-param) for Surface (1), for Modes (j=1,2,Nmode),	0.28734E+01	-0.24189E+01
Inertial Coupling (H-param) for Surface (2), for Modes (j=1,2,Nmode),	0.65518E+01	-0.31975E+01
Inertial Coupling (H-param) for Surface (3), for Modes (j=1,2,Nmode),	0.64592E+01	0.27719E+01
Inertial Coupling (H-param) for Surface (4), for Modes (j=1,2,Nmode),	0.29671E+01	0.22707E+01
Inertial Coupling (H-param) for Surface (5), for Modes (j=1,2,Nmode),	0.10041E+00	-0.67174E+01

FORCE/ MOMENT COEFFICIENTS DUE TO MODAL DISPLACEMENTS (ETA) - NON DIMENSIONAL

Cy due to Generalized Displacement eta(j), {Cy_eta(j)}, where (j=1,2,3,,Nmode)	-0.91586E-05	-0.38911E-03
Cz due to Generalized Displacement eta(j), {Cz_eta(j)}, where (j=1,2,3,,Nmode)	-0.71568E-07	-0.10300E-05
Cl (roll) due to Generalized Displacement eta(j), {Cl_eta(j)}, where (j=1,2,3,Nmode)	0.35548E-06	0.65812E-04
Cm (ptch) due to Generalized Displacement eta(j), {Cm_eta(j)}, where (j=1,2,3,Nmode)	0.74382E-08	0.50080E-07
Cn (yaw) due to Generalized Displacement eta(j), {Cn_eta(j)}, where (j=1,2,3,Nmode)	0.24838E-04	0.35673E-03

MODAL EXCITATION COEFFIC. DUE TO VEHICLE ROTATION: (alpha, beta, p,q,r)

Ceta(j) due to change in alpha, (Ceta(j)_alpha), (1/rad), where (j=1,2,.. n modes)...	-0.13497E-05	0.85751E-05
Ceta(j) due to change in beta, (Ceta(j)_beta), (1/rad), where (j=1,2,.. n modes)...	-0.21035E-03	-0.22198E-01
Ceta(j) due to roll rate (p), (Ceta(j)_p), (1/rad/sec), where (j=1,2,.. n modes)...	0.32655E-05	0.27380E-02
Ceta(j) due to pitch rate (q), (Ceta(j)_q), (1/rad/sec), where (j=1,2,.. n modes)...	-0.77263E-05	0.19004E-03
Ceta(j) due to yaw rate (r), (Ceta(j)_r), (1/rad/sec), where (j=1,2,.. n modes)...	-0.14193E-02	0.21156E-01

MODAL EXCITATION COEFFICIENTS DUE TO OTHER MODAL DISPLACEMENTS (Etas) - NON DIMENSIONAL

Ceta(1) due to Mode eta(j), {Ceta(i)_eta(j)}, for (j=1,2,.. n modes).....	0.27416E-08	0.44621E-07
Ceta(2) due to Mode eta(j), {Ceta(i)_eta(j)}, for (j=1,2,.. n modes).....	-0.11715E-07	0.17773E-06
Ceta(3) due to Mode eta(j), {Ceta(i)_eta(j)}, for (j=1,2,.. n modes).....	0.16304E-08	0.20609E-06
Ceta(4) due to Mode eta(j), {Ceta(i)_eta(j)}, for (j=1,2,.. n modes).....	-0.28338E-08	-0.55094E-07
Ceta(5) due to Mode eta(j), {Ceta(i)_eta(j)}, for (j=1,2,.. n modes).....	-0.35759E-08	-0.73494E-07
Ceta(6) due to Mode eta(j), {Ceta(i)_eta(j)}, for (j=1,2,.. n modes).....	-0.28094E-06	0.88503E-05
Ceta(50) due to Mode eta(j), {Ceta(i)_eta(j)}, for (j=1,2,.. n modes).....	-0.70602E-06	0.29796E-03

MODAL EXCITATION COEFFICIENTS DUE TO CONTROL SURFACE DISPLACEMENTS Delta(k) in (rad) - NON DIMENSIONAL

Ceta(1) due to Surface delta(j), {Ceta(i)_delt(j)}, (1/rad), for (j=1,2,Nsurface)	0.83492E-05	0.48124E-04
Ceta(2) due to Surface delta(j), {Ceta(i)_delt(j)}, (1/rad), for (j=1,2,Nsurface)	-0.39698E-03	-0.21795E-02
Ceta(3) due to Surface delta(j), {Ceta(i)_delt(j)}, (1/rad), for (j=1,2,Nsurface)	0.14720E-03	0.72046E-03
Ceta(4) due to Surface delta(j), {Ceta(i)_delt(j)}, (1/rad), for (j=1,2,Nsurface)	-0.29321E-04	-0.15488E-03
Ceta(5) due to Surface delta(j), {Ceta(i)_delt(j)}, (1/rad), for (j=1,2,Nsurface)	-0.10688E-04	-0.57579E-04
Ceta(6) due to Surface delta(j), {Ceta(i)_delt(j)}, (1/rad), for (j=1,2,Nsurface)	-0.40453E-02	-0.23649E-01
Ceta(50) due to Surface delta(j), {Ceta(i)_delt(j)}, (1/rad), for (j=1,2,Nsurface)	0.26426E-02	-0.13389E-02

HINGE MOMENT COEFFICIENTS DUE TO VEHICLE MOTION (Change in alpha,beta, p,q,r) - NON DIMENSIONAL

Hinge Moment at Surf(1) due to (alfa,beta,p,q,r), {Ch_alfa,Ch_beta,Ch_p,Ch_q,Ch_r}	-0.14979E+00	-0.27663E-01
Hinge Moment at Surf(2) due to (alfa,beta,p,q,r), {Ch_alfa,Ch_beta,Ch_p,Ch_q,Ch_r}	-0.79503E-01	0.34136E-01
Hinge Moment at Surf(3) due to (alfa,beta,p,q,r), {Ch_alfa,Ch_beta,Ch_p,Ch_q,Ch_r}	-0.78676E-01	-0.34546E-01
Hinge Moment at Surf(4) due to (alfa,beta,p,q,r), {Ch_alfa,Ch_beta,Ch_p,Ch_q,Ch_r}	-0.14927E+00	0.27672E-01
Hinge Moment at Surf(5) due to (alfa,beta,p,q,r), {Ch_alfa,Ch_beta,Ch_p,Ch_q,Ch_r}	-0.76125E-04	0.24899E+01

HINGE MOMENTS COEFFICIENTS DUE TO MODAL DISPLACEMENTS (Eta) - NON DIMENSIONAL

Hinge Moment at Surface (i= 1), due to Modes (j=1,2,3,,Nmode), {Ch(i)_eta(j)}	-0.14097E-06	-0.32901E-05
Hinge Moment at Surface (i= 2), due to Modes (j=1,2,3,,Nmode), {Ch(i)_eta(j)}	-0.64099E-06	-0.51432E-05
Hinge Moment at Surface (i= 3), due to Modes (j=1,2,3,,Nmode), {Ch(i)_eta(j)}	0.64689E-06	0.51864E-05
Hinge Moment at Surface (i= 4), due to Modes (j=1,2,3,,Nmode), {Ch(i)_eta(j)}	0.14169E-06	0.32839E-05
Hinge Moment at Surface (i= 5), due to Modes (j=1,2,3,,Nmode), {Ch(i)_eta(j)}	0.36458E-06	0.18191E-04

HINGE MOMENTS COEFFICIENTS DUE TO SURFACE DEFLECTIONS Delta(j) in (rad) - NON DIMENSIONAL

Hinge Moment at Surface (i= 1) due Surf. Deflect(j=1,2,3,,Nsurf), {Ch(i)_delt(j)}	-0.49590E+00	-0.11643E+00
Hinge Moment at Surface (i= 2) due Surf. Deflect(j=1,2,3,,Nsurf), {Ch(i)_delt(j)}	-0.20967E+00	-0.72956E+00
Hinge Moment at Surface (i= 3) due Surf. Deflect(j=1,2,3,,Nsurf), {Ch(i)_delt(j)}	-0.86948E-02	-0.18272E-01
Hinge Moment at Surface (i= 4) due Surf. Deflect(j=1,2,3,,Nsurf), {Ch(i)_delt(j)}	-0.27410E-02	-0.44335E-02
Hinge Moment at Surface (i= 5) due Surf. Deflect(j=1,2,3,,Nsurf), {Ch(i)_delt(j)}	0.56964E-02	0.12198E-01

FORCE/ MOMENT COEFFICIENTS DUE TO MODAL RATES (Eta_Dot) - NON DIMENSIONAL

Cy due to Modal Displacement Rate eta_dot, {Cy_eta(j)_dot}, where (j=1,2,3,, Nmode)	0.13938E-01	-0.23549E+00
Cz due to Modal Displacement Rate eta_dot, {Cz_eta(j)_dot}, where (j=1,2,3,, Nmode)	-0.21827E-03	0.32916E-05
Cl (roll) due to Modal Displ Rate eta_dot, {Cl_eta(j)_dot}, where (j=1,2,3,, Nmode)	-0.10518E-02	0.38271E-01
Cm (ptch) due to Modal Displ Rate eta_dot, {Cm_eta(j)_dot}, where (j=1,2,3,, Nmode)	-0.14474E-04	0.40727E-03
Cn (yaw) due to Modal Displ Rate eta_dot, {Cn_eta(j)_dot}, where (j=1,2,3,, Nmode)	0.15653E-02	0.10921E-01

MODAL EXCITATION COEFFIC. DUE TO VEHICLE RATES: (alpha_dot, beta_dot, p_dot, q_dot, r_dot)

Ceta(j) due to alpha_dot, (Ceta(j)_alpha_dot), (1/rad/sec), for (j=1,2,.. n modes)...	0.19118E-04	-0.84713E-03
Ceta(j) due to beta_dot, (Ceta(j)_beta_dot), (1/rad/sec), for (j=1,2,.. n modes)...	-0.14672E-04	-0.44200E-01
Ceta(j) due to roll accelerat (p_dot), (Ceta(j)_pdot), (1/rad/sec2), (j=1,2,n modes).	0.31664E-06	0.60499E-03
Ceta(j) due to pitch accelerat (q_dot), (Ceta(j)_qdot) (1/rad/sec2), (j=1,2,n modes).	0.97832E-05	-0.41204E-03
Ceta(j) due to yaw accelerat (r_dot), (Ceta(j)_rdot), (1/rad/sec2), (j=1,2,n modes).	-0.12173E-02	-0.38031E-01

```

MODAL EXCITATION COEFFICIENTS DUE TO MODAL RATES (Eta_dot) -NON DIMENSIONAL
Ceta( 1) due to Mode Rate eta(j)_dot, {Ceta(i)_eta(j)_dot}, for (j=1,2,.. Nmodes).. -0.29782E-06 -0.19582E-05
Ceta( 2) due to Mode Rate eta(j)_dot, {Ceta(i)_eta(j)_dot}, for (j=1,2,.. Nmodes).. 0.32548E-04 -0.72432E-03
Ceta( 3) due to Mode Rate eta(j)_dot, {Ceta(i)_eta(j)_dot}, for (j=1,2,.. Nmodes).. -0.20360E-04 0.16462E-03
Ceta( 4) due to Mode Rate eta(j)_dot, {Ceta(i)_eta(j)_dot}, for (j=1,2,.. Nmodes).. 0.28421E-05 -0.28605E-04
Ceta( 5) due to Mode Rate eta(j)_dot, {Ceta(i)_eta(j)_dot}, for (j=1,2,.. Nmodes).. 0.77741E-06 0.87210E-05
Ceta( 50) due to Mode Rate eta(j)_dot, {Ceta(i)_eta(j)_dot}, for (j=1,2,.. Nmodes).. 0.80768E-03 -0.31422E-02

MODAL EXCITATION COEFFICIENTS DUE TO CONTROL SURFACE RATES (Delta_dot) in (rad/sec) - NON DIMENSIONAL
Ceta( 1) due to Surface Rate delta(j)_dot, {Ceta(i)_delt(j)_dot}, (1/rad/sec)..... -0.19894E-04 0.12222E-04
Ceta( 2) due to Surface Rate delta(j)_dot, {Ceta(i)_delt(j)_dot}, (1/rad/sec)..... 0.13740E-02 0.40367E-03
Ceta( 3) due to Surface Rate delta(j)_dot, {Ceta(i)_delt(j)_dot}, (1/rad/sec)..... -0.67040E-03 -0.95475E-03
Ceta( 4) due to Surface Rate delta(j)_dot, {Ceta(i)_delt(j)_dot}, (1/rad/sec)..... 0.10841E-03 0.85585E-04
Ceta( 5) due to Surface Rate delta(j)_dot, {Ceta(i)_delt(j)_dot}, (1/rad/sec)..... 0.32719E-04 0.22192E-04
Ceta( 50) due to Surface Rate delta(j)_dot, {Ceta(i)_delt(j)_dot}, (1/rad/sec)..... 0.89602E-02 0.20782E-01 -
HINGE MOMENT COEFFICIENTS DUE TO VEHICLE RATES (Rates of alpha,beta, p,q,r) - NON DIMENSIONAL
Hinge Moment at Surface ( 1), due to Rate of alpha,beta,p,q,r, Ch_alpha_dot, etc. -0.53297E+00 -0.30159E-01
Hinge Moment at Surface ( 2), due to Rate of alpha,beta,p,q,r, Ch_alpha_dot, etc. -0.54079E+00 -0.12020E+00
Hinge Moment at Surface ( 3), due to Rate of alpha,beta,p,q,r, Ch_alpha_dot, etc. -0.56556E+00 0.12791E+00 -
Hinge Moment at Surface ( 4), due to Rate of alpha,beta,p,q,r, Ch_alpha_dot, etc. -0.53202E+00 0.32859E-01 -
Hinge Moment at Surface ( 5), due to Rate of alpha,beta,p,q,r, Ch_alpha_dot, etc. 0.18525E-02 0.17513E+01

HINGE MOMENTS COEFFICIENTS DUE TO MODAL RATES (Eta_dot) - NON DIMENSIONAL
Hinge Moment at Surface (i= 1), due to Modal Rates (j=1,2,3..), {Ch(i)_eta(j)_dot} 0.76625E-05 -0.13242E-02
Hinge Moment at Surface (i= 2), due to Modal Rates (j=1,2,3..), {Ch(i)_eta(j)_dot} -0.11396E-03 -0.24421E-02
Hinge Moment at Surface (i= 3), due to Modal Rates (j=1,2,3..), {Ch(i)_eta(j)_dot} 0.11593E-03 0.26397E-02
Hinge Moment at Surface (i= 4), due to Modal Rates (j=1,2,3..), {Ch(i)_eta(j)_dot} -0.87002E-05 0.13396E-02
Hinge Moment at Surface (i= 5), due to Modal Rates (j=1,2,3..), {Ch(i)_eta(j)_dot} -0.97202E-04 0.10498E-01

HINGE MOMENTS COEFFICIENTS DUE TO SURFACE RATES Delta_dot(k) in (rad/sec) - NON DIMENSIONAL
Hinge Moment at Surface (i= 1) due to Surf. Rates (j=1,2,3..), {Ch(i)_delt(j)_dot} -0.31012E+01 -0.24992E+00
Hinge Moment at Surface (i= 2) due to Surf. Rates (j=1,2,3..), {Ch(i)_delt(j)_dot} -0.56626E+00 -0.36149E+01
Hinge Moment at Surface (i= 3) due to Surf. Rates (j=1,2,3..), {Ch(i)_delt(j)_dot} 0.35358E-02 -0.38872E-02
Hinge Moment at Surface (i= 4) due to Surf. Rates (j=1,2,3..), {Ch(i)_delt(j)_dot} 0.81291E-02 0.45393E-02
Hinge Moment at Surface (i= 5) due to Surf. Rates (j=1,2,3..), {Ch(i)_delt(j)_dot} 0.47320E-02 0.16826E-01
-----

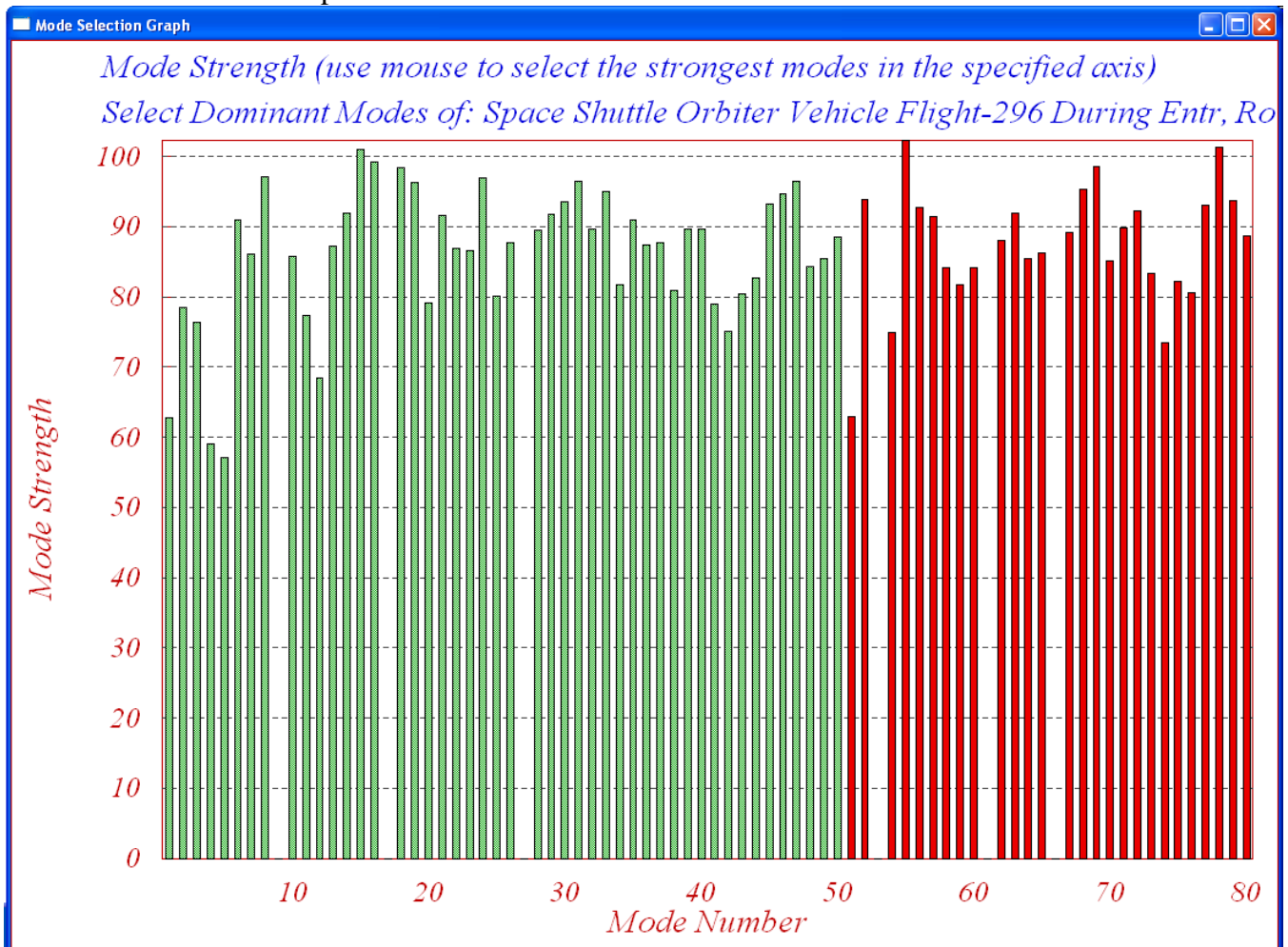
```

2.3 Selecting the Flex Modes

Before we use the FVMP, process the input data and create the flex orbiter dynamic model, however, we must also describe how we selected the modes. That is, the selected set of 50 modes, already discussed, which is inside the input data file “*Shuttle-Entry-Flx.Inp*”. The title of the selected modes set is “*Shuttle Early Hypersonic Atmospheric Re-Entry, First 50 Modes*”. These modes will eventually be combined with the vehicle and GAFD data to create the flexible state-space model. Notice that an input file may contain more than one set of selected modes with different titles for different applications, but in this case the file “*Shuttle_Entry_Flx.Inp*” contains only one set of 50 modes. The title of the selected modes should also be included in the bottom line of the vehicle data set, below the line “Number of Modes: 50”, in order for the vehicle modeling program to be able to associate the modal data with the vehicle data. A question may be asked, why is it necessary to go through mode selection if we already know that we will use only the first 50 modes that correspond to the 50 GAFD frequencies? The answer is that we still have to use the mode selection process because it allows us to scale the data, plus, we must also select nodes that correspond to vehicle locations, such as: gyros and accelerometer sensors, reaction jets, surface hinges, etc.

Start the Flixan program and go to directory: “*C:\Flixan\Examples\Shuttle Hypersonic Re-Entry\Flex_Analysis*”. From the main menu select: “*Program Functions*”, then “*Flight Vehicle/Spacecraft Modeling Tools*”, and then “*Flex Mode Selection*” to start the mode selection program. Click “*Continue*” on the introduction. Select the vehicle data, modal data, and node files, as shown. Also select the default output file that creates a list of mode strength versus mode frequency for all modes. From the following menu select the title of the only vehicle input data-set “*Shuttle Orbiter Flex Model for Early Re-Entry*” and click on “*Run Input Set*”.

are selected the color of the mode bars changes after selection, from red to green. Press “Enter” when the mode selection is complete.



Enter Notes

Enter some notes describing the mode selection criteria, excitation points, directions, etc. To be used for future reference

The first 50 modes were selected from all three: roll, pitch, and yaw axes

In the field below the analyst may finally write a short description that provides information about what the mode selection. Explaining, for example, the reasoning behind the choices made, such as, conditions, actuator and sensor locations, forcing directions, etc. The user notes will be included as comment lines in the selected modes set, below the title. The selected mode frequencies and shapes are finally saved in file “*Shuttle_Entry_Flx.Inp*”. The default title of the modal set was modified to: “*Shuttle Early Hypersonic Atmospheric Re-Entry, First 50 Modes*”.

2.5 Linear Flex Stability Analysis

The Simulink model “*Anal_6Dof.mdl*” in Figure (23) is used to perform linear frequency domain stability analysis. It is located in folder “...*Examples\Shuttle Hypersonic Re-Entry\Flex-Analysis\Mat-Analysis*”, and consists of the flexible vehicle system, actuators, sensors, and flight control system in series. On the right side, the RCS and the aero-surface loops are expanded from vectors and they can manually be wired by opening and closing the proper loops for frequency response analysis one loop at a time. The aero-surfaces control system consists of three (roll, pitch, yaw) loops. The RCS consists of four loops (p, q, r, and Nz) control assuming continuous thrusters. The Simulink model can be modified by closing and opening the various loops as needed, according to the loop to be analyzed. The system should be able to demonstrate good stability characteristics in both pitch and lateral, and under three operating conditions, (a) aero-surfaces operating without RCS, (b) RCS operating without aero-surfaces, and (c) when RCS and aero-surface loops are operating in parallel. All these conditions must be checked separately using the Simulink model in Figure (23).

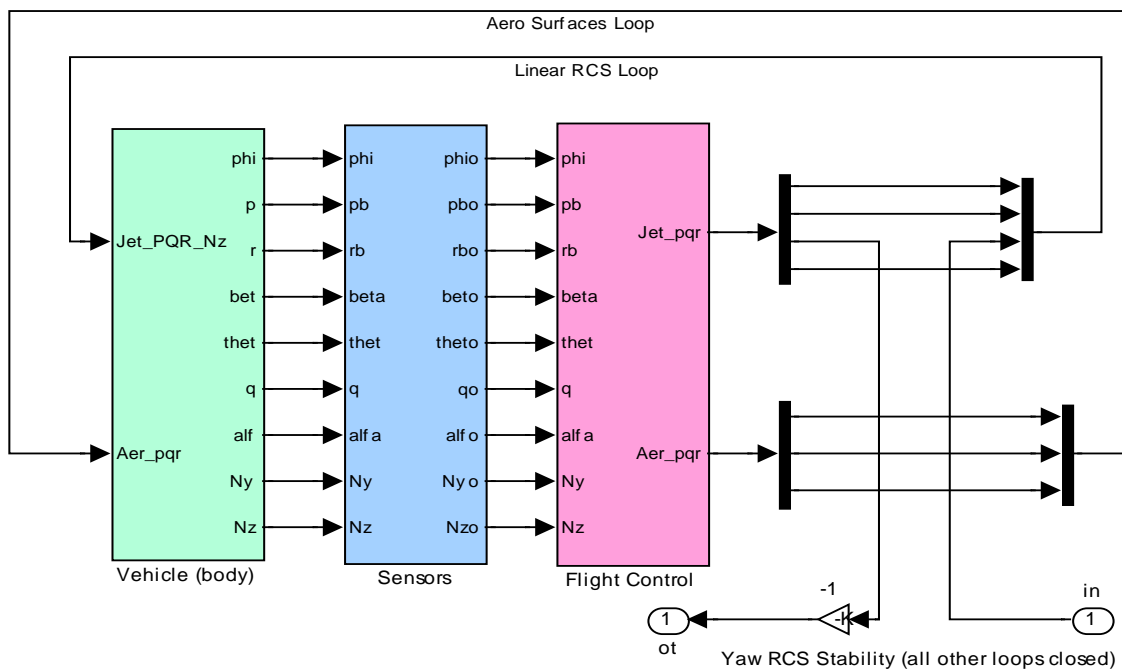


Figure (23) Simulink Model “*Anal_6Dof.mdl*” for Frequency Domain Stability Analysis

For example, in order to check yaw axis stability of the RCS system when the aero-surfaces control system is closed, we close all three surface loops. We also close the (roll, pitch, and Nz) RCS feedback loops and open only the yaw loop, as shown in Figure (23). Then we calculate the frequency response across the open yaw loop, which is shown in Figure (33). For a more efficient stability analysis and limit-cycling evaluation a Describing Function analysis of the non-linearities is required, but this is beyond our present scope. The file “run.m” loads the systems, gains and filters, it creates a SISO system from the modified “*Anal_6Dof.mdl*” model, and calculates the frequency response across the opened loop. But before we get into the frequency domain analysis let us first take a look at the three main blocks in figure (23): the flex vehicle, the actuators, the sensors, and the flight control system.

Vehicle Block

The flex vehicle block is shown in detail in figure (24). In the center of the diagram there is a state-space system of the Flexan generated flexible vehicle system “*Space Shuttle Orbiter Flex Model during Early Re-Entry*” from file “*Shuttl-Entry-Flx.Qdr*”. This system was converted to a function “*vehi_6dof_flx.m*” for Matlab analysis. This diagram also includes the jet-selection logic block that was described in the rigid-body modeling. The jet select logic uses the RCS mixing logic matrix “*KJmix*”, a Matlab function “*Pos_Thrust3.m*”, and a block of pulse-width-modulators to calculate the multi-level throttle commands (0 to 1) for the 11 thrusters. Notice that the jet-selection logic is only used in the 6-dof model. For linear analysis the jet-selection block in “*Anal_6Dof.mdl*” is replaced with the mixing logic matrix *KJmix*. This subsystem also includes an actuator block that contains five distinct actuators for each aero-surface. The actuators provide acceleration outputs for the aero-surface TWD/ Inertial coupling dynamics implementation. There is also closed a mechanical hinge-moments feedback loop that applies load-torques on the actuators coming from the vehicle hinge-moment outputs. There is also a shaped wind-gust disturbance which is applied to the last input #27 and represents a 50 (ft/sec) gust. The direction of the gust is defined in the vehicle input data.

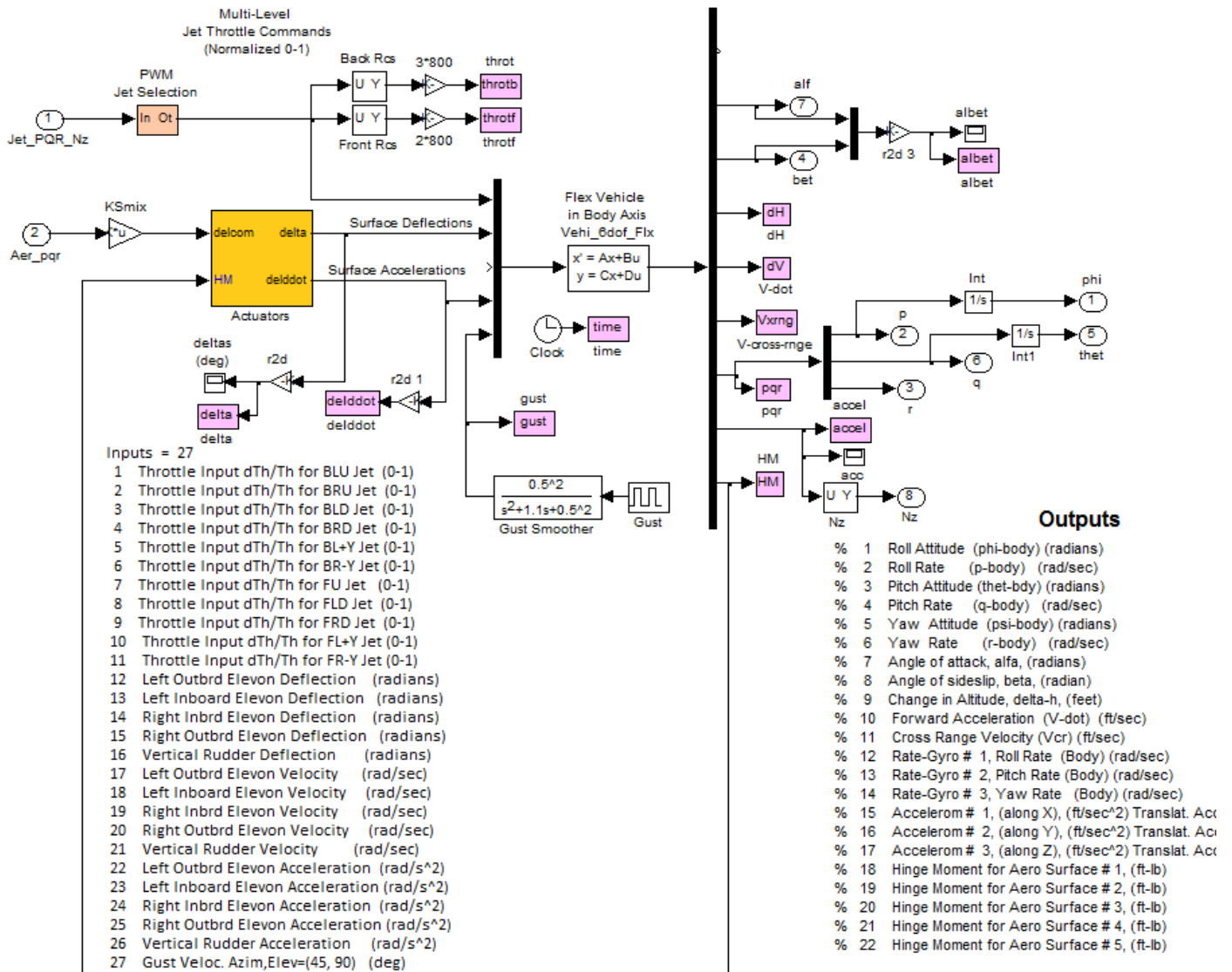


Figure (24) Subsystem Consisting of Flexible Vehicle, RCS & Surface Mixing Logic and Actuators

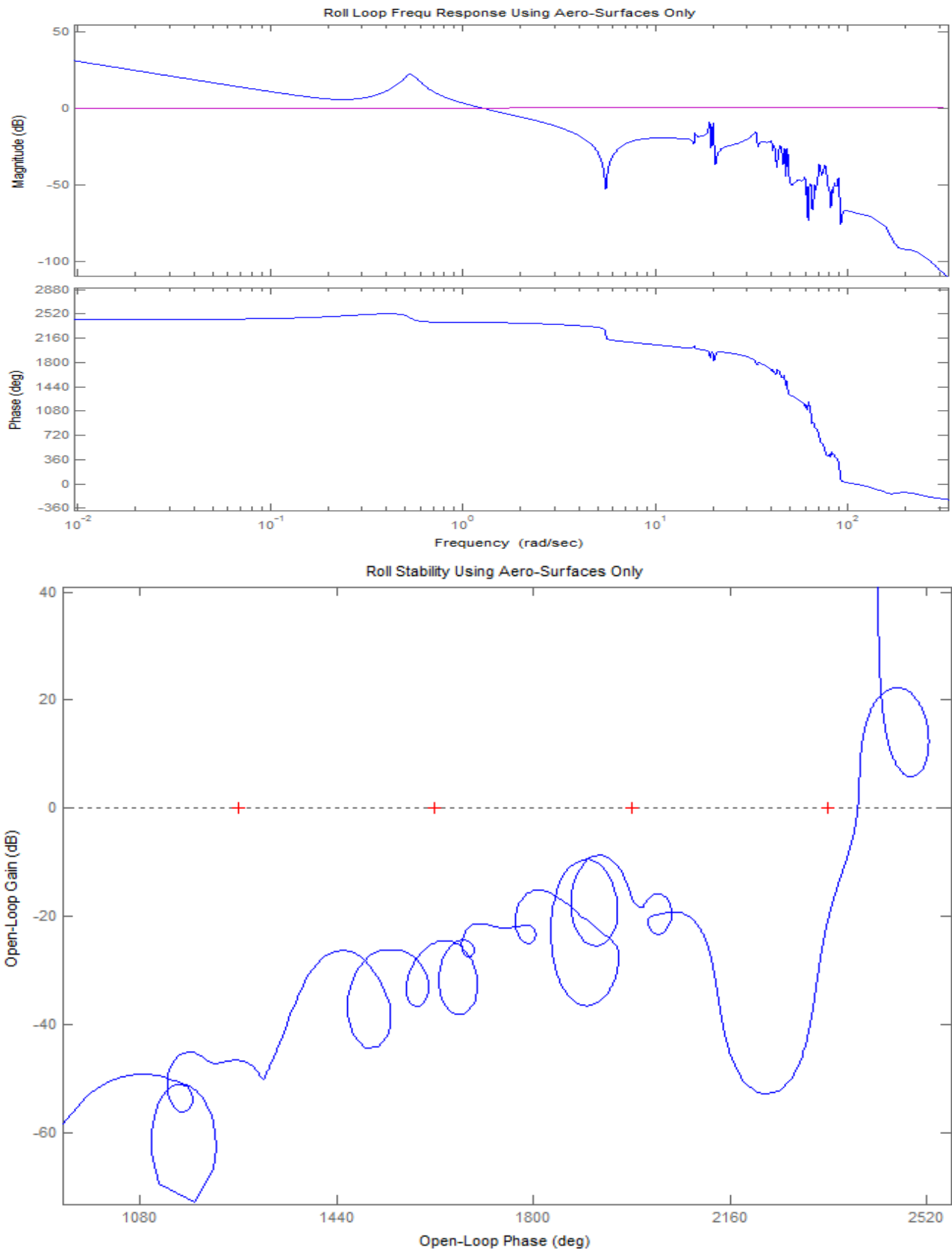


Figure (30) Roll axis Stability Analysis Using Aero-Surfaces Only, the RCS loop is Opened

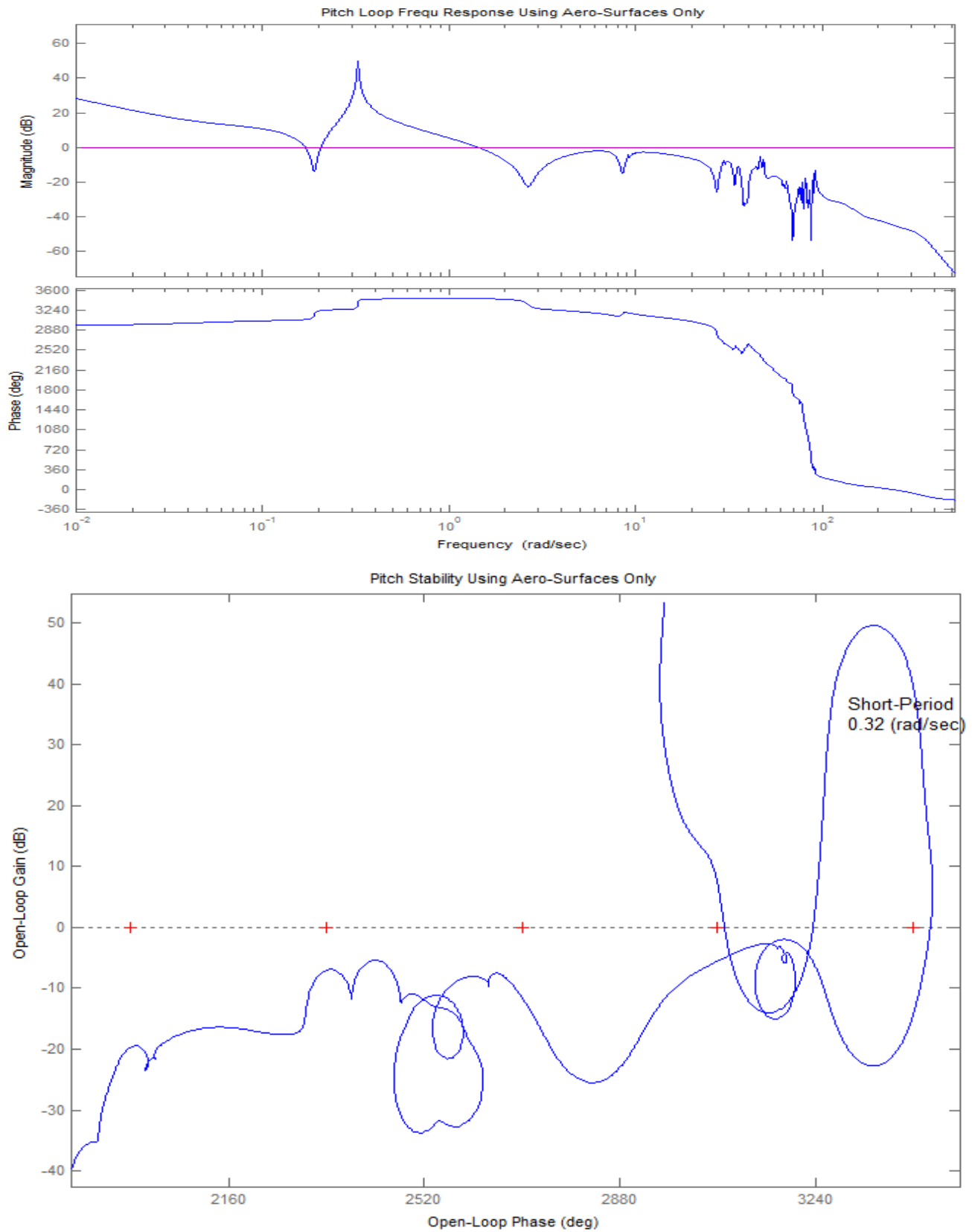


Figure (31) Pitch axis stability using aero-surfaces only, the RCS loop is opened. It shows a lightly damped phugoid mode (18 deg phase-margin), and a rigid-body phase-margin of 34 (deg). All flex modes are gain stabilized.

2.7 Time Domain Simulation

The Simulink model “*Sim_6Dof_pwm.mdl*” in Figure (34) is used to simulate the flexible vehicle non-linear response to commands and to gust excitations. It is located in subdirectory “\Examples \Shuttle Hypersonic Re-Entry \Flex-Analysis\Mat-Analysis” and it is similar to the rigid-body simulation. It consists of the same blocks as the frequency domain flex model, but all loops are closed. The jet mixing matrix KJ_{mix} , however, is replaced with the PWM/ multi-level RCS thrusting logic as already described in the rigid model.

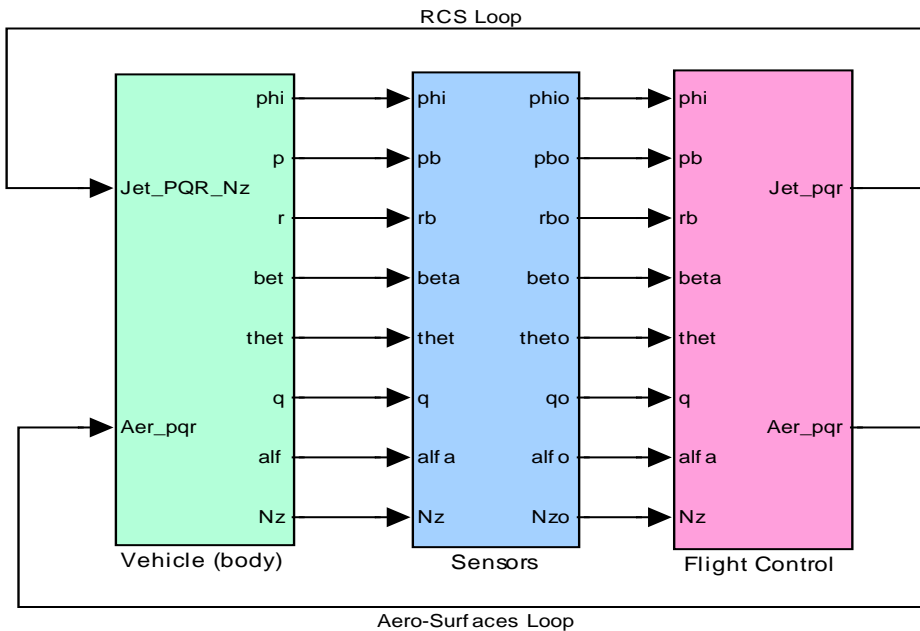
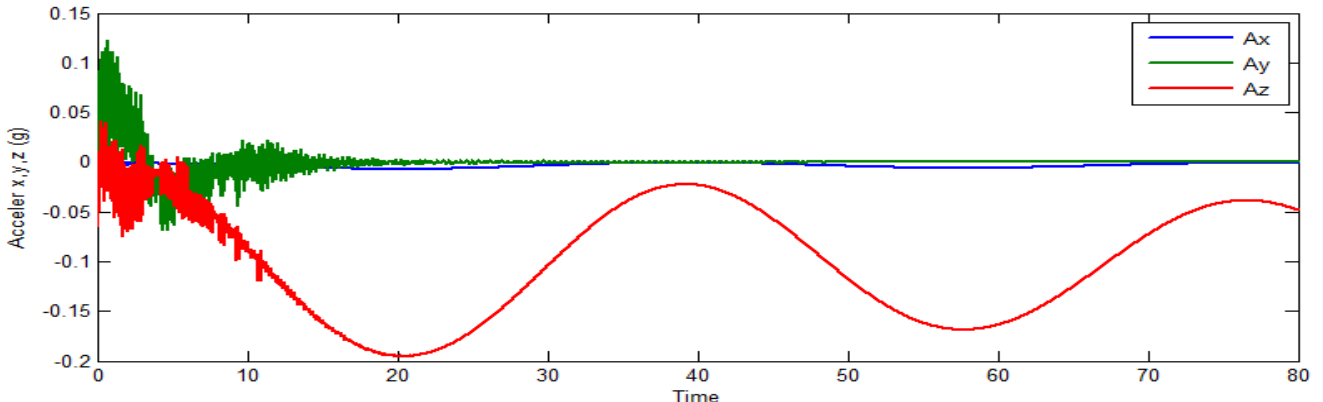
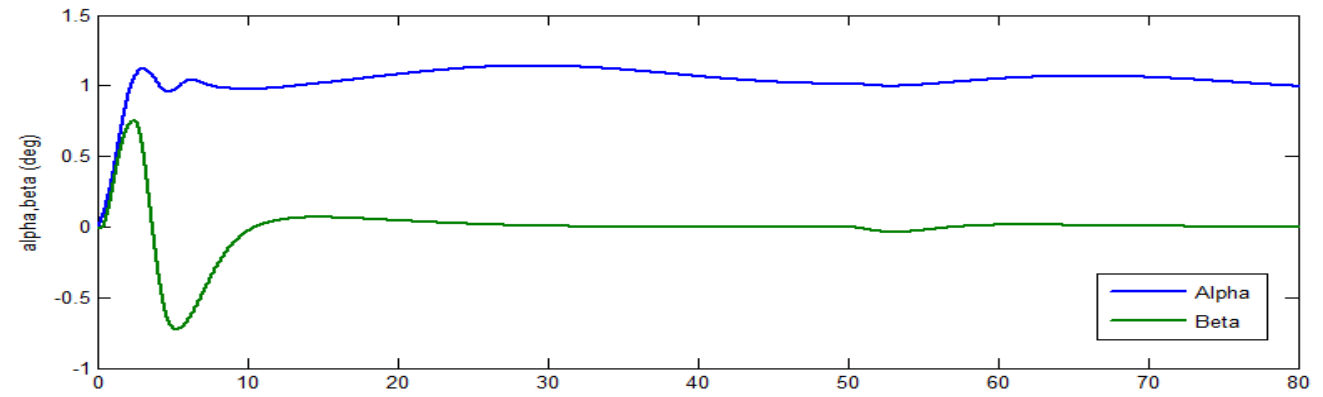
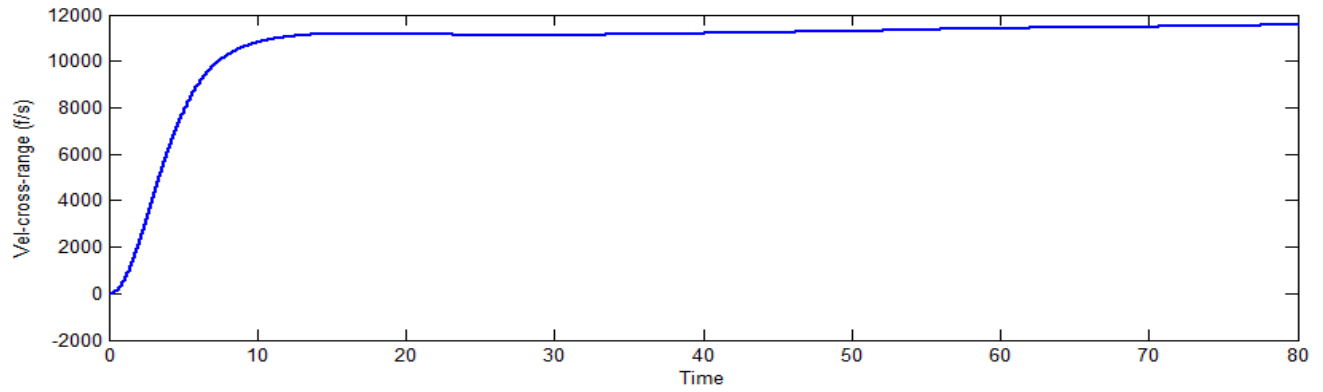
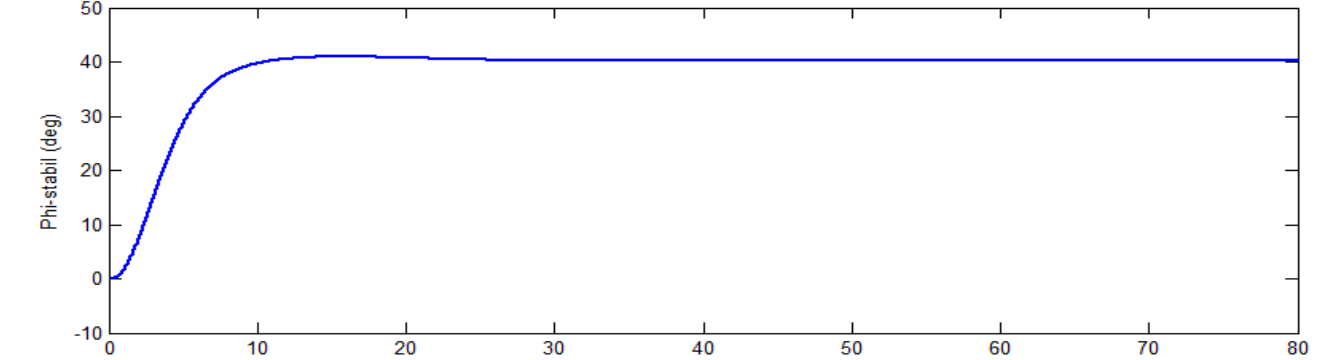


Figure (34) Flex-Vehicle Closed-Loop Simulation Model “*Sim-6Dof_pwm.mdl*”

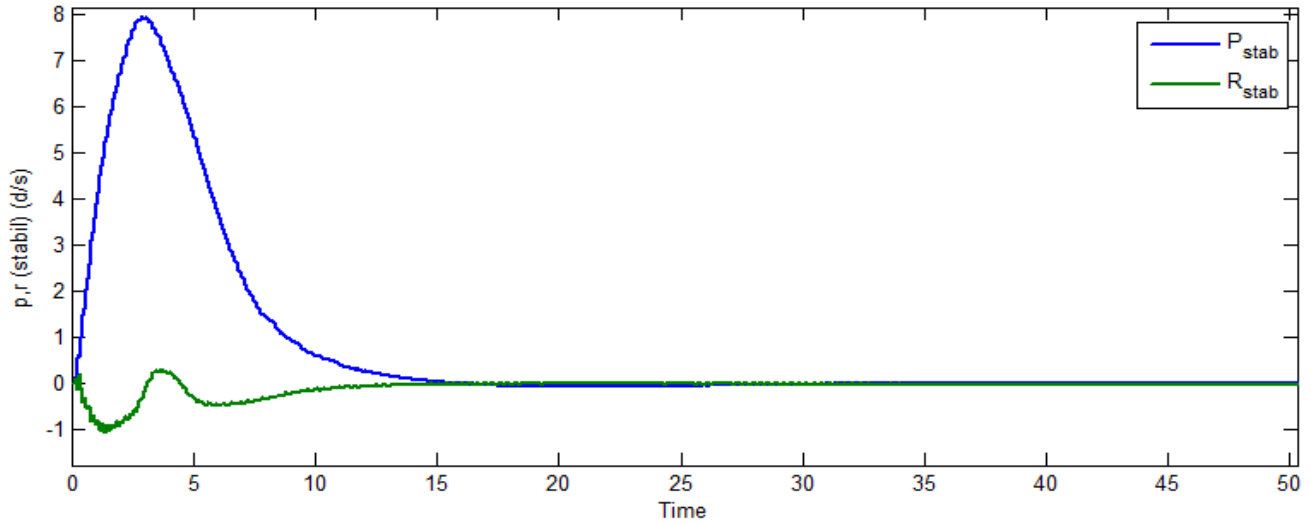
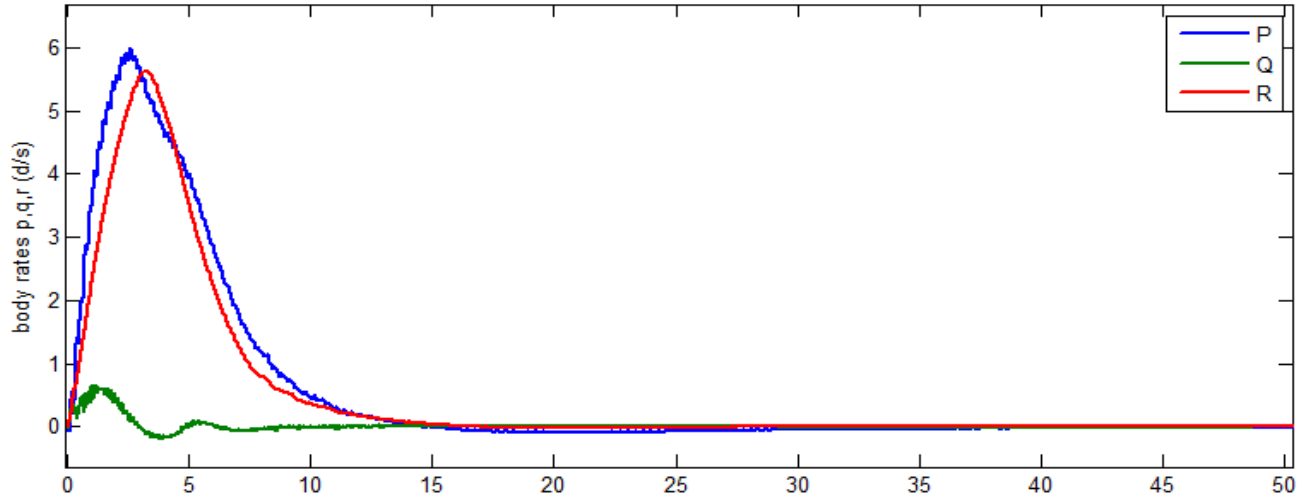
Similar to the rigid-body simulation, the above Simulink model will be used to simulate the response of the vehicle to simultaneous 1° pitch step command, 40° roll step command about the velocity vector, and a 50 (ft/sec) filtered wind-gust pulse. The direction of the gust is defined in the vehicle input data. The initialization file “run.m” loads the systems, matrices, control system gains and filters for the simulation. The file “pl.m” plots the simulation results. as shown below. The vehicle responds to the pitch and roll guidance commands with very little coupling in (β). The roll rate is mainly in p-stability, that is, about the velocity vector as commanded to minimize sideslip. The bank angle causes a steady cross-range velocity. The small low frequency oscillation superimposed on alpha is due to the lightly damped phugoid mode which is excited by the pitch command. The phugoid is also visible in the Nz acceleration and causes altitude and velocity oscillations. The figures also show the multi-level PWM thruster firing activity separately in the front and in the rear RCS pods. The 3-level rear thrusters produce a maximum of 2400 (lb) thrust, and the 2-level front thrusters produce a maximum of 1600 (lb) thrust. The thrusts are in multiples of 800 (lb). The thrust oscillations occurring between two firing levels are pulse-width modulated to produce the demanded average acceleration. Overall, the plots are similar to the rigid-body simulations.



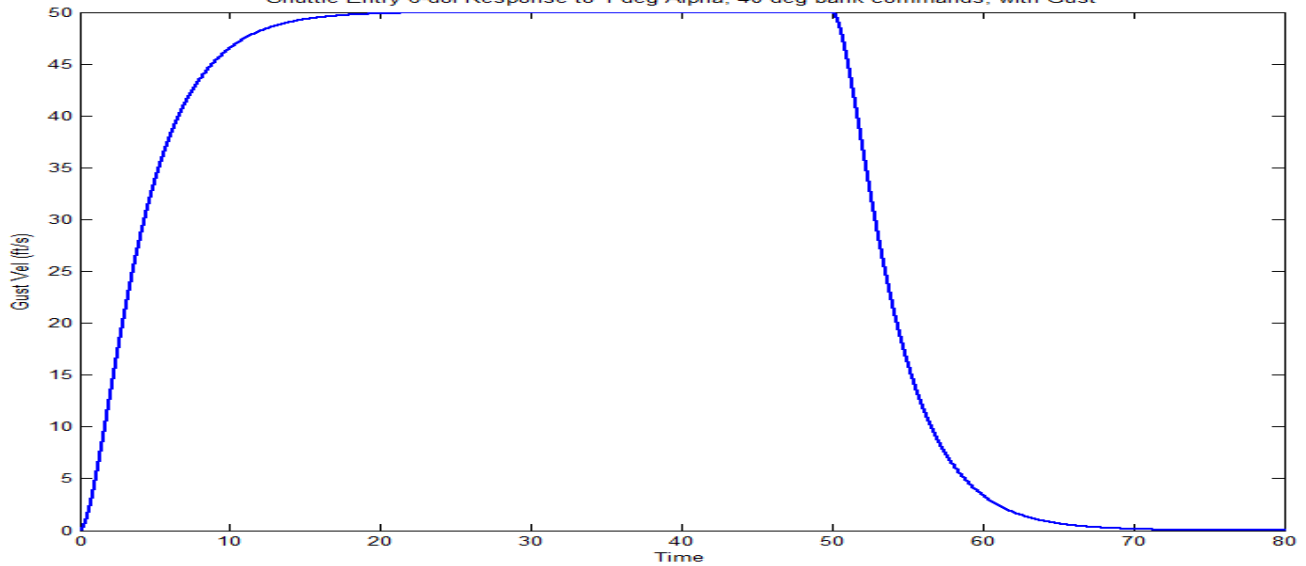
Shuttle Entry 6-dof Response to 1 deg Alpha, 40 deg bank commands, with Gust

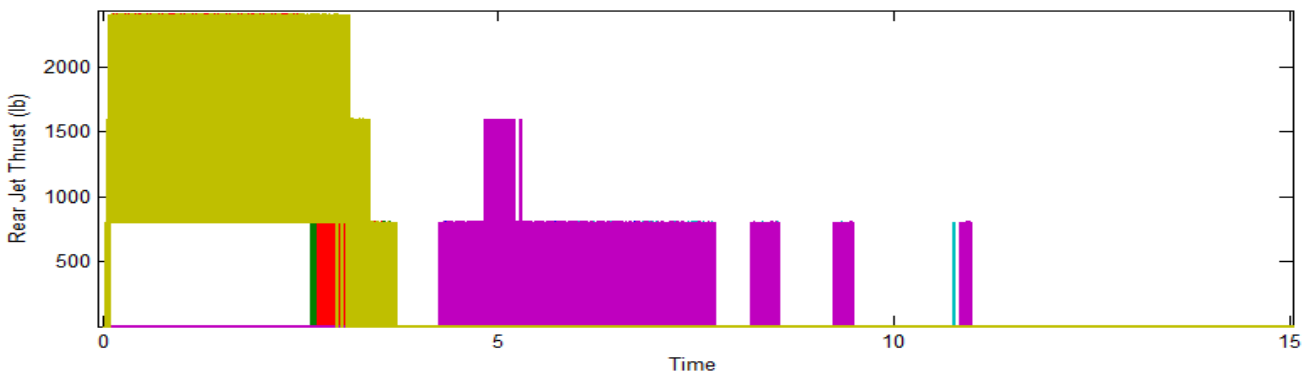
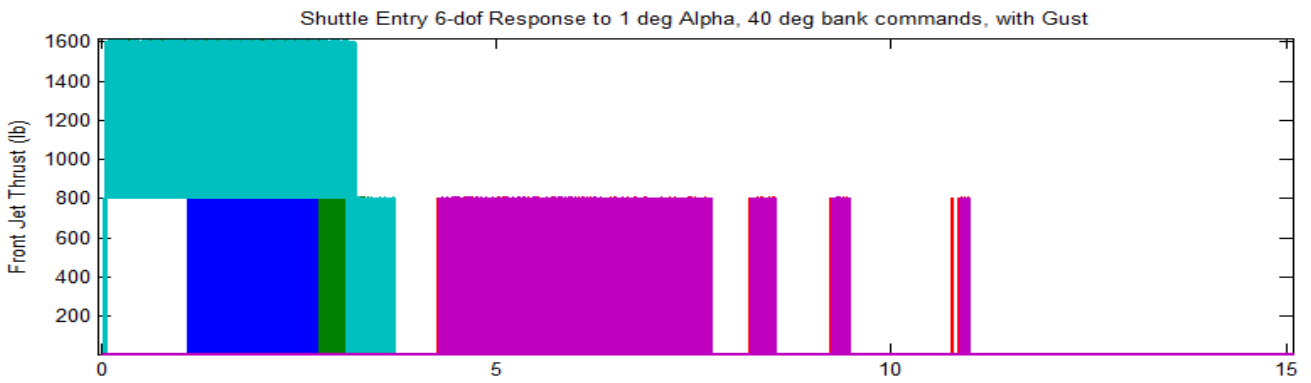
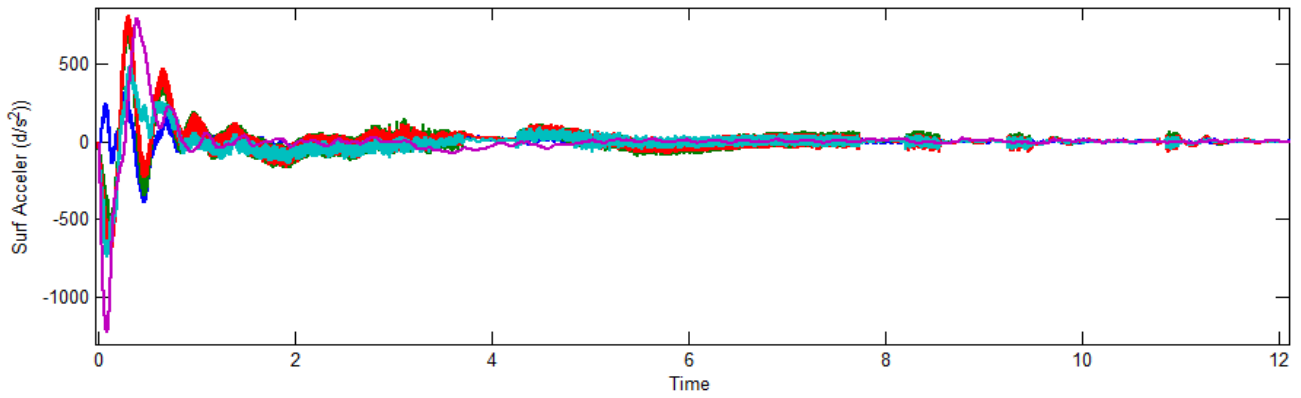
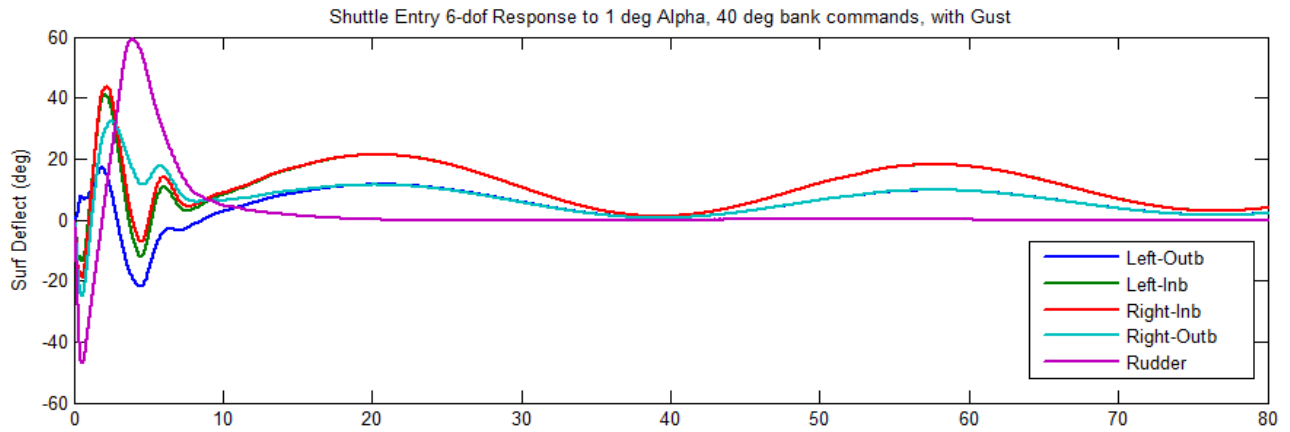


Shuttle Entry 6-dof Response to 1 deg Alpha, 40 deg bank commands, with Gust



Shuttle Entry 6-dof Response to 1 deg Alpha, 40 deg bank commands, with Gust





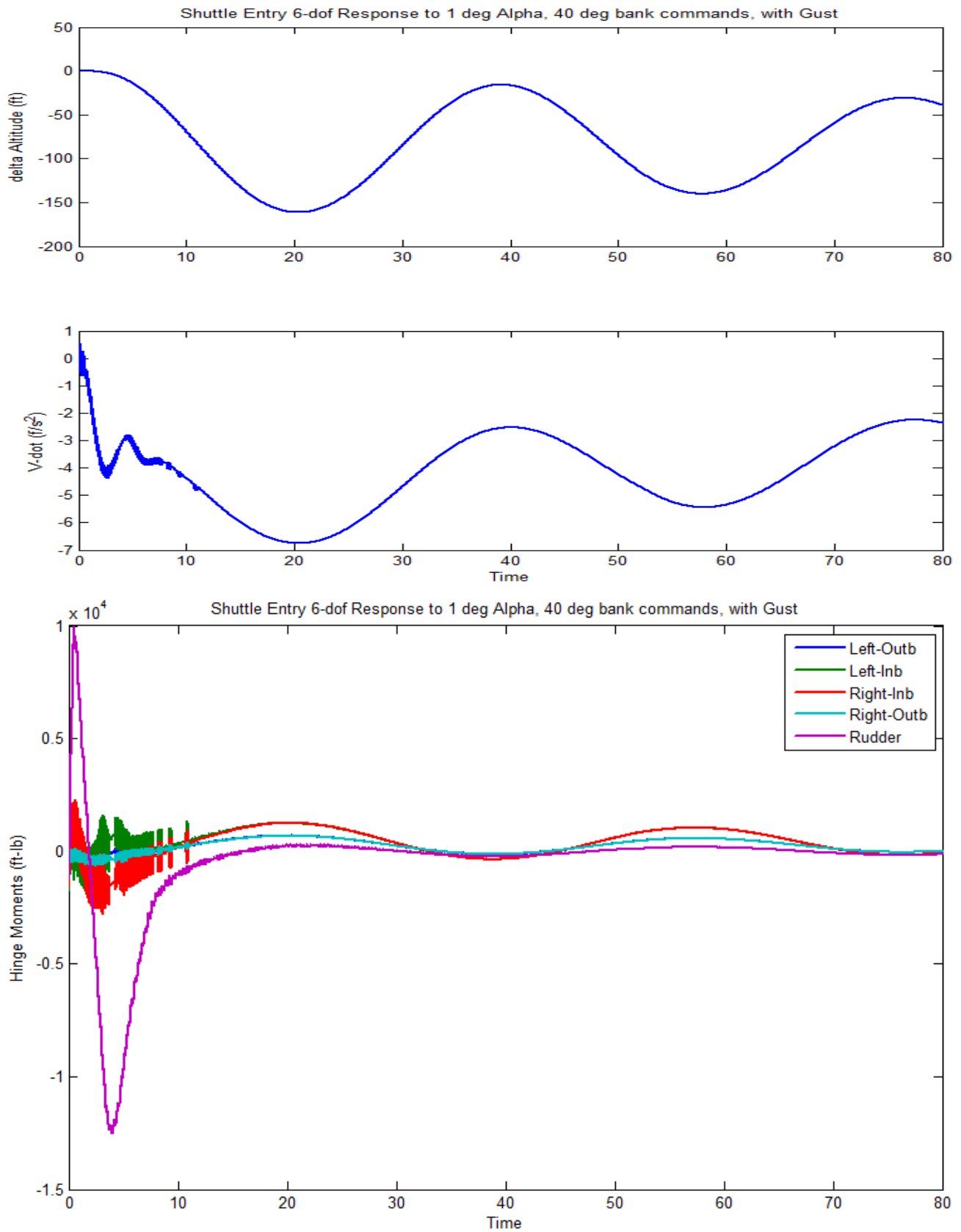


Figure (14g) Hinge moments at the control surfaces. The Rudder experiences significantly larger hinge moments than the inboard and outboard Elevons